A comprehensive experimental and modeling study of npropylcyclohexane oxidation

Mingxia Liu, Ruozhou Fang, Chih-Jen Sung, Khalid Aljohani, Aamir Farooq, Yousef Almarzooq, Olivier Mathieu, Eric L Petersen, Philippe Dagaut, Jie Zhao, et al.

A comprehensive experimental and modeling study of n-propylcyclohexane oxidation

Mingxia Liu[1], Ruozhou Fang[2], Chih-Jen Sung[2], Khalid Aljohani[3], Aamir Farooq[3], Yousef Almarzooq[4], Olivier Mathieu[4], Eric L. Petersen[4], Philippe Dagaut[5], Jie Zhao[6], Zhiping Tao[6], Lijun Yang[7], Chong-Wen Zhou*[1,8]

[1]School of Energy and Power Engineering, Beihang University, Beijing 100191, PR China

[2]Department of Mechanical Engineering, University of Connecticut, Storrs, CT 06269, USA

[3]King Abdullah University of Science and Technology, Clean Combustion Research Center, Physical Sciences and Engineering Division, Thuwal 23955, Saudi Arabia

[4]J. Mike Walker ’66 Department of Mechanical Engineering, Texas A&M University, College Station, TX 77843, United States

[5]Laboratoire de Combustion et Systèmes Réactifs, CNRS, 1C, Avenue de la Recherche Scientifique, 45071 Orléans Cedex 2, France

[6]Research Institute of Petroleum Processing, Sinopec, 18 Xueyuan Road, Haidian District, Beijing 100083, PR China

[7]School of Astronautics, Beihang University, Beijing 100191, PR China

[8]Combustion Chemistry Centre, School of Chemistry, Ryan Institute, National University of Ireland, Galway, Galway H91TK33, Ireland.

E-mail address: cwzhou@buaa.edu.cn (C.-W. Zhou)

Abstract:

n-Propylcyclohexane (nPCH) is an important surrogate component for jet fuel, gasoline, and diesel. To comprehensively understand its combustion properties and chemical kinetics, ignition delay time (IDT) measurements of nPCH/air mixtures were performed in a high-pressure shock tube (HPST) at fuel-rich conditions (φ = 2.0), pressures of 10–40 bar and temperatures of 738–1400 K. Also, low-temperature IDT measurements were carried out in a rapid compression machine (RCM) at a pressure of 10 bar, temperatures of 615–750 K, and equivalence ratios of 0.5–2.0. In addition, laminar flame speeds were measured at an initial temperature of 403 K, at pressures of 1.01 bar and 3.04 bar, and equivalence ratios ranging from 0.7 to 1.4.

A detailed chemical kinetic mechanism has been developed in the current work to describe the oxidation of nPCH, including 10 high-temperature reaction classes and 24 low-to-intermediate temperature reaction classes. Important reactions were identified by sensitivity and flux analyses at different temperatures, pressures, and equivalence ratios. These reaction classes play a very important role in determining the fuel reactivity and the distribution of products. This model shows good agreement with the experiment measurements carried out in this work and the ones in the literature, including IDTs, species data from jet-stirred reactor and flow reactor experiments, and laminar flame speeds.

Keywords: *n-Propylcyclohexane oxidation; Chemical kinetic modeling; Shock tube; Rapid compression machine; Laminar flame speed; Jet-stirred reactor.*

1.Introduction

Cycloalkanes are a significant class of hydrocarbons in transportation fuels, accounting for up to approximately 35% in conventional diesel fuel, about 20% in jet fuel, and about 10% in gasoline [1]. The combustion properties of cycloalkanes are unique, especially for their low-temperature chemistry which is different from those of n-alkanes and olefins. In particular, the negative temperature coefficient (NTC) behavior of cycloalkanes is more pronounced than that of olefins, but less than that of n-alkanes [2]. Also, the high concentration of cycloalkanes in real fuel would raise soot emissions because they can dehydrogenate and produce aromatics, which are thought to be inception sites for soot growth [3]. Therefore, understanding the pyrolysis and oxidation of cycloalkanes is also important for accurately predicting the sooting behavior of real fuels. n-Propylcyclohexane (nPCH) is selected as a promising component which can help attain a good match for these kerosene properties. For example, Dagaut et al. [4] chose nPCH as one of the surrogate components for Jet A-1 fuel and its molar fraction in the surrogate mixture is 0.11.

The oxidation and pyrolysis of n-propylcyclohexane have been investigated in both experimental and kinetic modeling studies in the literature, and most of these studies focused on intermediate- and high-temperature conditions as summarized in Table 1 along with the corresponding pressures, equivalence ratios (φ), and reactant compositions. Previous experimental investigations on nPCH include global combustion properties such as ignition delay times (IDTs) [5-8], laminar flame speeds [5, 9], and ignition temperature [10]. Also, concentration profiles of species in pyrolysis [11], oxidation [6, 12-14], and flames [15] of nPCH have been measured. These experiments provided different types of validation datasets to help developing a comprehensive model of nPCH. However, there is still a lack of IDTs at low temperatures, high pressures, and fuel-rich condition (φ = 2.0) and laminar flame speeds at high pressure. Fundamental datasets under these conditions are important because of their direct relevance with respect to the kerosene and fuel-rich engine technologies. Furthermore, these newly-acquired experimental results from various facilities provide multiple model validation targets which allow more rigorous model development practice.

Meanwhile, kinetic models for nPCH oxidation and pyrolysis have been developed previously [5, 6, 11, 12, 15-17]. However, most of those literature models focused on the intermediate-to-high temperature chemistry of nPCH, and hence the modeling efforts at low-to-intermediate temperatures are meager. Moreover, the conformer difference of nPCH is expected to play a critical role in its oxidation process, as it would lead to distinct reaction pathways and the resulting products. Those important aspects have not been considered in the literature models, thereby motivating the present study.

In view of the above, as an important aviation fuel surrogate component, the oxidation mechanism of nPCH has not been studied comprehensively over wide temperature and pressure ranges relevant to engine conditions. In the current work, a detailed chemical kinetic model including low- to high-temperature chemistry has been developed to describe n-propylcyclohexane oxidation. Sensitivity and flux analyses

were performed to identify these important reaction classes. New IDTs for nPCH oxidation were acquired in both a shock tube and a rapid compression machine over the temperature range of 615–1400 K and a pressure range of 10–40 bar with equivalence ratios of 0.5–2.0 in air. In addition, laminar flame speeds were measured at unburnt gas temperature of T = 403 K, at initial pressures of 1.01 bar and 3.04 bar, and equivalence ratios of 0.7-1.4. The model developed in this study has been validated against a wide range of experimental data from this work and those in the literature [5, 6, 9, 11-15], including IDTs, laminar flame speeds, and species concentrations from experiments of jet-stirred reactor (JSR) and flow reactor (FR).

Table 1
List of literature experimental data for n-propylcyclohexane pyrolysis and oxidation.

Experiment	Initial conditions			Reactant composition %			
	T (K)	p (bar)	φ	nPCH	O_2	Bath gas	Reference
Shock tube IDT	1250-1800	10-20	0.2-1.5	0.0075-0.1	0.45-6.8	93.1-99.5 (Ar)	Dubois et al. [5]
Shock tube IDT	1110-1650	1.11	0.5-1.5	0.5	3.375-13	86.5-96.125 (Ar)	Tian et al. [7]
Shock tube IDT	740-1120	20, 40	0.5, 1.0	0.77	20.85	78.38 (N_2)	Ahmed et al. [6]
RCM IDT	620-895	20, 40	0.5, 1.0	1.53	20.69	77.78 (N_2, CO_2)	Ahmed et al. [6]
RCM IDT	620-930	4.5-13.4	0.3-0.5	0.47-0.77	20.84-20.9	N_2, Ar, CO_2	Crochet et al. [8]
Laminar flame speed	403	1.0	0.6-1.75	0.96-2.63	20.44- 20.81	76.93- 78.25(N_2)	Dubois et al.[5]
Laminar flame speed	353	1.01	0.7-1.5	1.08-2.30	20.53-20.77	77.17-78.16(N_2)	Ji et al. [9]
Flame ignition	373	1.01		1-10	-	90-99 (N_2)	Liu et al. [10]
Flame species	333	0.067	0.68	0.81nPCH	36.8	44.71 (Ar)	Pousse et al. [15]
				7.1 methane			
Flow reactor	950-1300	0.04, 1.0		0.5	-	He, Kr	Wang et al. [11]
Jet-stirred reactor	950-1250	1.01	0.5-1.5	0.1	0.9-2.7	97.2-99 (N_2)	Ristori et al. [12]
Pressurized flow reactor	550-850	8.0	0.27	0.0826	4.21	95.7074 (N_2)	Ahmed et al. [6]
Jet-stirred reactor	550-800	1.01	0.5-2.0	0.5	3.4-13.5	86-96.1 (N2)	Ahmed et al. [6]
Jet-stirred reactor	800-1200	10.13	0.5-2.0	0.05-0.1	0.45-1.35	98.6-99.5 (N_2)	Mati et al. [13]
Jet-stirred reactor	550-950	10.13	0.25	0.1	5.4	94.5 (N_2)	Diévart et al. [14]

2. Experimental and simulation methods

2.1. Experimental methods

2.1.1. University of Connecticut (*UConn*) *rapid compression machine*

Measurements of IDTs for nPCH/air mixtures were performed in a heated RCM, consisting of a cylindrical reaction chamber, a piston arrangement, a hydraulic chamber, a pneumatic chamber, and a driving tank. As the detailed RCM description can be found in [18, 19], a brief overview is given here. The premixed nPCH/air mixtures in this study were prepared in a heated stainless-steel mixing tank, which is connected to the reaction chamber by a heated manifold. A reactive mixture was prepared at room temperature by filling the pre-vacuumed mixing tank with nPCH, O_2, and N_2 one at a time. As nPCH is liquid at room temperature, a glass syringe was used to inject the fuel

into the mixing tank first. Then O_2 and N_2 were filled into the mixing tank consecutively based on barometric measurements. For "air", the molar ratio of N_2/O_2 is kept at 3.76. After filling the reactants, the heaters, and the magnetic stirrer at the bottom of mixing tank were switched on. Typically, 4 hours can completely vaporize the liquid fuel as well as stabilize the initial temperature (T_0) and ensure homogeneity of the mixture. High purity nPCH (99%, Sigma-Aldrich) and high purity O_2 and N_2 (>99.99%, Airgas) were used to prepare the test mixtures. The molar proportions of the reactive mixtures and the corresponding test conditions investigated here are summarized in Table 2.

Table 2
Summary of test conditions for nPCH/air mixtures (in molar %) used in the current RCM experiments.

Mix#	φ	nPCH	O_2	N_2	p_c (bar)
1	0.5	0.77	20.85	78.38	10
2	1.0	1.53	20.69	77.78	10
3	2.0	3.02	20.37	76.61	10

As nPCH used in this RCM study has high purity (99%, Sigma Aldrich) and the original nPCH container comes with a rubber septa seal which prevents excessive gas entry over time, the influences of impurity species on experimental results are deemed negligible, so the fuel was not degassed before being used. In each experiment, the premixed nPCH/air mixture was first filled to the reaction chamber and then rapidly compressed by the piston to reach a specific elevated pressure and temperature condition at the end of compression (EOC). The piston arrangement is pneumatically driven and hydraulically stopped, with a crevice to suppress the vortex roll-up effect to ensure homogeneity during and after compression. The EOC temperature (T_C) and pressure (p_c) can be changed independently by varying the overall compression ratio, initial pressure (p_0), and T_0 of each experiment. The primary diagnostic on the RCM was the in-cylinder dynamic pressure measured by a Kistler 6125C pressure transducer. To characterize the facility effect (i.e., the heat transfer effect [20]) on the reactive experiment and to confirm that there was no exothermicity during the compression stroke, the corresponding non-reactive experiment was also conducted by replacing O_2 in the reactive mixture with N_2. Fig. 1 shows a raw experimental pressure trace for nPCH/air ignition obtained by the RCM, as well as the definitions of the IDTs. The definitions of τ_1 and τ are the time interval from the EOC to the respective maximum of the first order time derivative of pressure (dp/dt). $\tau_1 = \tau_1$ is the first-stage IDT and τ_2 is the second-stage IDT. As such, $\tau = \tau_1+\tau_2$ is the total IDT for this two-stage ignition case. At least four consecutive runs were taken for each experimental condition to ensure repeatability. The typical scatters of τ_1 and τ were less than 15% of the reported values. The raw pressure dataset was processed by UConnRCMPy [21], which is a Python package used to determine p_c, T_C, and IDT(s). In UConnRCMPy, T_C was calculated using $\int_{T_0}^{T_C} \gamma dT/(\gamma-1)T = \ln(p_c/p_0)$, where γ is the temperature-dependent specific

heat ratio. The detailed information about T_C calculation as well as the use of non-reactive pressure trace to characterize the facility effect can be found in [22, 23].

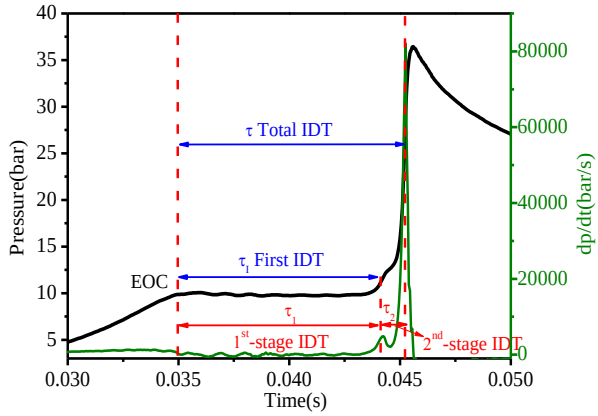

Fig. 1. Example of nPCH/air ignition delay time measurement from the UConn RCM at T_C = 692 K, p_c = 10 bar, φ = 1.0.

2.1.2. King Abdullah University of Science and Technology (KAUST) shock tube

IDT measurements of n-propylcyclohexane were also conducted using the High-Pressure Shock Tube (HPST) facility at KAUST. The driver and driven sections of the shock tube are separated by a mid-section where two pre-scored aluminum diaphragms are used to generate the desired shock waves. The shock tube is made of stainless steel and has an inner diameter of 10 cm. To prevent fuel condensation, the shock tube, mixing vessel and mixing manifold were heated to 90–100 °C. The incident shock speed was measured using six dynamic pressure transducers placed towards the end of the driven section. Temperature and pressure behind reflected shock waves, (T_5, p_5), were calculated using one-dimensional shock-jump relations. IDT was determined using pressure and OH* chemiluminescence signals measured at a location 1 cm away from the endwall. Uncertainty in T_5 and p_5 is estimated to be <1% and the uncertainty in IDTs is ~ 15–20%. Prior to use, n-PCH was degassed by freeze-pump-thaw cycles. nPCH mixtures were prepared by injecting the liquid fuel into an evacuated mixing vessel with subsequent complete evaporation. After fuel injection, high-purity gasses were supplied to the vessel in the sequence of N_2 (99.9998%) and O_2 (99.9997%). Mixtures were stirred for ~ 4–6 hours before the experiments to ensure homogeneity.

The oxidation of n-propylcyclohexane in air was examined over three pressures (10, 20, and 40 bar), temperatures from 738 to 1400 K, and an equivalence ratio of 2.0. The measurements at relatively lower temperatures, where IDTs are longer than ~ 2 ms, were carried out by tailoring the driver gas (helium) with up to 10% N_2. IDT from this shock tube is presented in Fig. 2. The measured reflected shock pressure profiles exhibited non-ideal pressure rise of approximately (dp/dt) ($1/p_0$) = 3%/ms at the studied conditions.

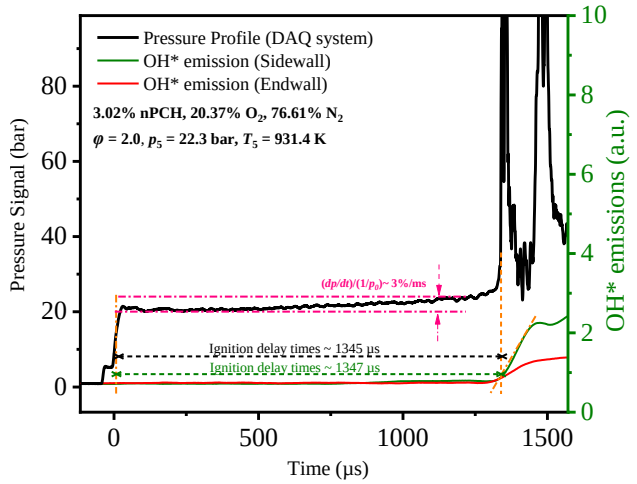

Fig. 2. Example of nPCH/air ignition delay time measurement from the KAUST HPST experiments at T_5 = 931.4 K, p_5 = 22.3 bar, φ = 2.0.

2.1.3. Laminar flame speed (TAMU)

A stainless-steel, constant-volume vessel designed for high-temperature, high-pressure laminar flame speed experiments was used at Texas A&M University (TAMU) in the current study. It can perform tests for up to 600 K initial temperature and 30.40-bar initial pressure. The constant-volume vessel is a cylinder with an internal diameter of 31.8 cm and a length of 28 cm. Optical diagnostics are accessible using the two opposed glass windows with a large diameter of 12.7 cm allowing for spherical flame tests at near-constant pressure. More details of the vessel are available in Krejci et al. [24]. A modified Z-type schlieren imaging system is used to capture the spherically propagating flame using a high-speed camera with a frame rate of 10,000 fps using a mercury lamp light source. Fig. 3 shows a sample experiment for the spherically propagating flame from the current study. An in-house Python code is then used to detect the flame-front edges, and the analysis is automatically carried out. An example of this edge-detection process is visible in Fig. 3. Finally, the laminar flame speed and Markstein Length are calculated using the non-liner equation investigated by Chen [25]. Fig. 4 illustrates burned-gas flame speed as a function of stretch for one of the cases investigated herein, and it can be seen how the confinement- and ignition-affected images are excluded in a typical test. The unstretched, burned-gas laminar flame speed is determined by extrapolating the trend in Fig. 4 to zero stretch. Subsequently, the unstretched, unburned laminar flame speed is calculated by multiplying the unstretched, burned-gas flame speed by the ratio of the burned-to-unburned gas densities obtained from a chemical equilibrium calculation [24]. The complete set of laminar flame speed values along with their corresponding Markstein Lengths are tabulated in the Supplementary Material (SMM).

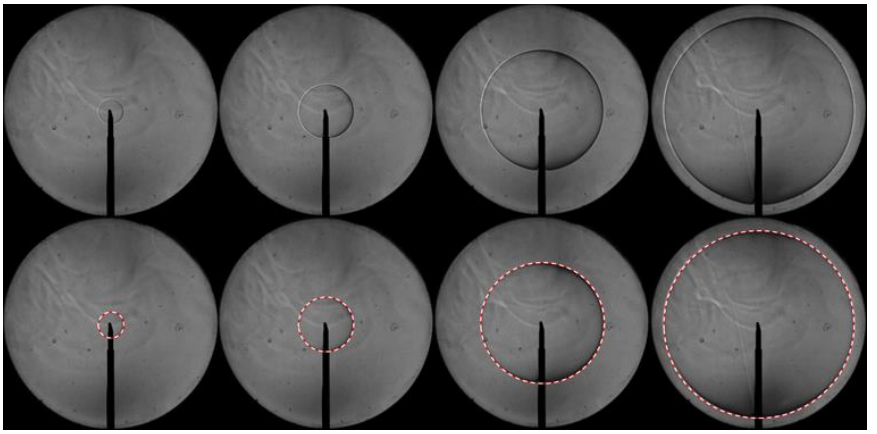

Fig. 3. Example of nPCH/air spherically propagating flame from a TAMU experiment at T_i = 403 K, P_i = 1.01 bar, φ = 0.87 along with edge detection (lower images) using an in-house Python code.

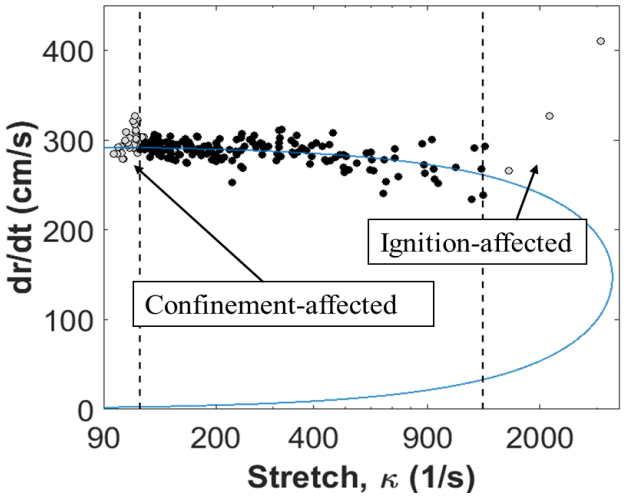

Fig. 4. Example of nPCH/air laminar flame speed determination from the stretched, burned-gas velocity (i.e., *dr/dt*) from a TAMU laminar flame experiment at T_i = 403 K, P_i = 1.01bar, φ = 1.34.

Fuel was introduced into the vessel by injection using a syringe with an accurately known mass (± 0.01 g) for each condition. Partial pressure of the fuel (PP_f) was then monitored using a 0-0.133 bar pressure transducer installed on the vessel. Following that, Primary Standard Air was filled to the desired initial pressure. During these experiments, an unusual behavior of the PP_f was observed for the nPCH. Immediately following fuel injection, the vessel pressure increased (as anticipated); however, within one minute, the PP_f started to drop, indicating a fuel condensation or adsorption issue. To investigate this issue, the reported vapor pressure of nPCH at 403 K was checked. According to [26], the vapor pressure of nPCH is about 0.49 bar at 403 K. All experiments in the current study were performed at 403 K, and the maximum partial pressure of nPCH during these experiments was only about 0.053 bar (for 3.04-bar initial pressure experiments). So, even for this extreme case, the partial pressure of nPCH was always below its vapor pressure by more than a factor of nine. In addition, the injected fuel mass (m_f) was plotted against PP_f and is shown to be perfectly linear in the SMM. Therefore, the facts that nPCH vapor pressure was much higher than the

PP_f during the experiments, coupled with the straight-line relation shown in the SMM between m_f and PP_f, indicate that the issue of decreasing PP_f was likely not due to condensation. We suspect that the apparent loss of nPCH in the vessel could be due to preferential adsorption of the fuel onto the steel walls or similar phenomenon. This reason was explained in detail in the SMM. Finally, it is worth mentioning that the fuel was not degassed prior to its introduction in the vessel. However, introducing the fuel with the syringe also removes the possibility of introducing gaseous air while the solubility of air in the fuel should be relatively low. No discrepancy between the fuel introduced in the vessel on a mass base and the subsequent pressure reading of the fuel in the vessel was observed. Any gas dissolved in the liquid fuel is therefore introduced at a level so low that a potential shift in the targeted mixture composition can be neglected, and its effect would be well below the other uncertainties affecting the results.

2.2. Simulation methods

2.2.1. Ignition delay time simulations

Ignition delay time simulations for the RCM data need to take the effect of machine specific effects (e.g., heat transfer effect) into consideration. The machine specific effects during and after compression were accounted for by the "adiabatic core expansion" approach [27-29], namely, the machine specific effects are modeled as reactor volume change. A combined pressure trace is used to deduce the reactor volume history. Specifically, the combined pressure trace uses the pressure profile during the compression stroke (before the EOC) from the reactive experiment, while the pressure profile after the EOC is taken from the corresponding non-reactive run. This is to ensure that the combined pressure trace faithfully captures the reactor condition during and after the compression stroke. Cantera is subsequently used to convert the combined pressure trace to the resulting volume history. The deduced volume history can be fed to zero-dimensional calculations to determine the simulated pressure trace, from which the simulated IDTs can be obtained. More details about the RCM simulation can be found in [23].

Shock tube ignition delay time simulations were carried out as zero-dimensional calculations. The non-ideal facility effect $(dp/dt)/(1/p_0)$ = 3%/ms was considered in the simulations. For simulations of IDTs from literature, the definition of IDT is taken consistently with that specified by each experiment.

2.2.2. Species simulations

The speciation simulations of the experimental data from jet-stirred reactor and flow reactor were performed in the current work. Temperature-distance profiles for the flow reactor experiments of [11] were used as input profiles in the simulations.

2.2.3. Brute-force sensitivity and flux analyses on nPCH autoignition

"Brute force" sensitivity analyses of IDT with respect to the reaction rate parameter were carried out to identify the key reactions controlling fuel reactivity. Assuming a constant reactor volume, the analyses were conducted by increasing and decreasing the A-factor of each reaction by a factor of two to compute the influence on the predicted

total ignition delay time.

The sensitivity coefficient is defined as : $S=\frac{\ln(\tau_+/\tau_-)}{\ln(k_+/k_-)}=\frac{\ln(\tau_+/\tau_-)}{\ln(2.0/0.5)}$,

where τ_+ (τ_-) is the total ignition delay time calculated using the increased (decreased) rate constant. A negative sensitivity coefficient indicates a reaction promoting reactivity and vice versa.

Flux analyses were carried out to identify the most important pathways of fuel consumption and to understand the final products at different temperature regions. They were performed at the time corresponding to 20% fuel consumption assuming a constant volume reactor.

2.2.4. Laminar flame speed simulations and sensitivity analyses

In order to avoid a high computational cost and time, a high-temperature version of the current mechanism was used to simulate laminar flame speeds, which was created by removing fuel low-temperature oxidation chemistry including all the associated species and relevant reactions. Laminar flame speed sensitivity analysis was performed which computes the first-order sensitivity coefficients for the predicted mass flow rate corresponding to the flame speed. A positive sensitivity coefficient indicates a reaction promoting reactivity and vice versa.

3. Chemical kinetic mechanism development

A detailed nPCH combustion chemistry mechanism has been developed hierarchically starting with the latest C0–C4 base chemistry from AramcoMech 3.0 [30-37] with some updated rate constants [38-40]. The nPCH sub-mechanism includes 10 high-temperature reaction classes and 24 low- to intermediate-temperature reaction classes recommend by [41-43]. The group additivity method developed by Benson [44] with some updated group values by Burke et al. [45] was used to calculate the thermodynamic parameters for all new species, which were performed utilizing the THERM program developed by Ritter and Bozzelli [46]. In addition, the Transport Data Estimator package of the Reaction Mechanism Generator software from Green et al. [47] has been used to provide relevant transport properties. The present comprehensive kinetic mechanism, thermochemistry, transport files and glossary are provided in the SMM. This model was analyzed by sensitivity and flux analyses to highlighted the crucial reaction classes which were discussed in Sections 3.1-3.6. It was also validated comprehensively against various experimental results from this work and literature which were presented in Section 4 and Figs. S4-S16 in SMM.

3.1. Important reactions classes highlighted

Key reactions for nPCH oxidation at different temperature regimes were highlighted by “brute force” sensitivity analyses for RCM and/or ST IDTs, flux analyses, and laminar flame speed sensitivity analysis. All reactions highlighted here are discussed in

detail in the following sections, and the scheme of reaction pathways are presented in Fig. 5.

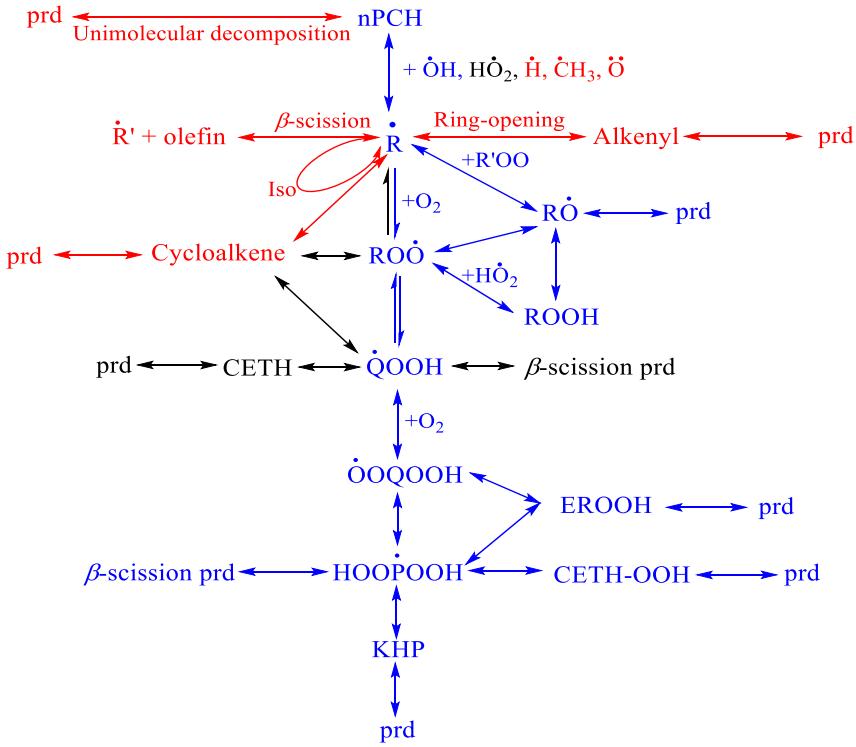

Fig. 5. Scheme of reaction pathways included in this work for nPCH oxidation. CETH: cyclic ether, EROOH: cyclic alkene-hydroperoxy, CETH-OOH: cyclic ether-hydroperoxy, KHP: cyclic keto-hydroperoxy, prd: products [48] (red: high-temperature; blue: low-temperature; black: NTC behavior).

3.2. Unimolecular decomposition

At high temperatures, nPCH pyrolysis starts with C–C/C–H bond breaking or isomerizing into different C9 alkene isomers by the ring-opening reactions, as shown in Fig. 6. All reactions were included in the current model, among which the sensitivity analysis in Fig. 7 shows that the reaction of NC_3H_7+cC_6H_{11} <=> $C_3H_7cC_6H_{11}$ promotes overall reactivity at T = 1300 K. There are no theoretical and experimental studies available in the literature for the reaction class shown in Fig. 6. The rate constants for the C–C bond decomposition of sidechain were estimated by analogy with those of alkanes [49] at the CASPT2/cc-pvdz//B3LYP/6-31G* level of theory with a correction from CAS+1+2+QC/aug-cc-pvtz calculation for CH_3+CH_3, while the rate constants for the ring-opening reactions were estimated by analogy with those of methylcyclohexane [50] at the MRCI/6-31+g(d,p)//CAS(6,6)/6-31+g(d,p) level of theory. The rate constants for the C–H bond fission reactions were estimated by analogy with those of alkanes [51] at the CASPT2/cc-pvdz level of theory combined with the variable reaction coordinate transition state theory with a dynamical correction (a factor of 0.9) from the CAS+1+2/aug-cc-pvtz calculation for H+CH_3.

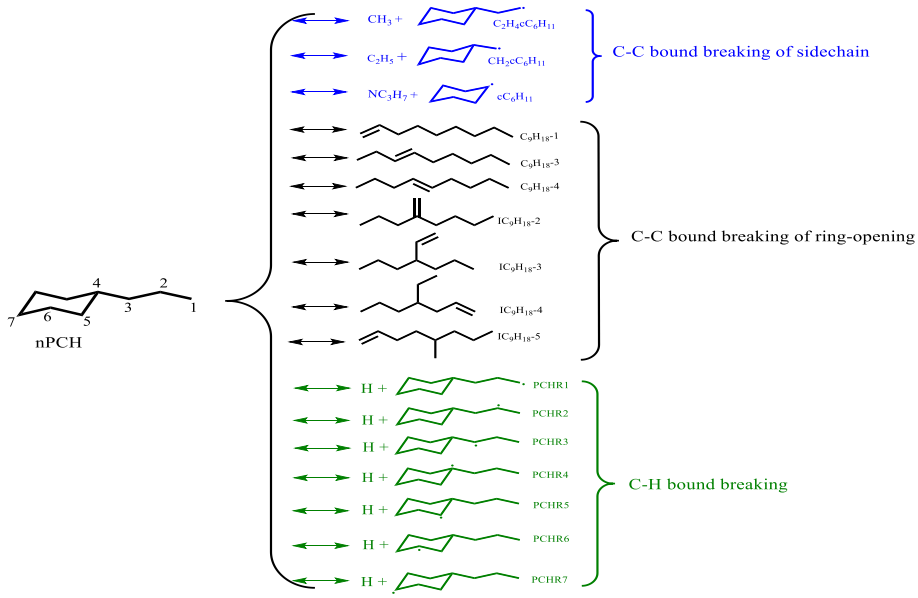

Fig. 6. Unimolecular decomposition reactions for nPCH included in the current model (blue: C–C bond breaking channels on the sidechain; black: C–C bond breaking channels on the ring; green: C–H bond breaking channels).

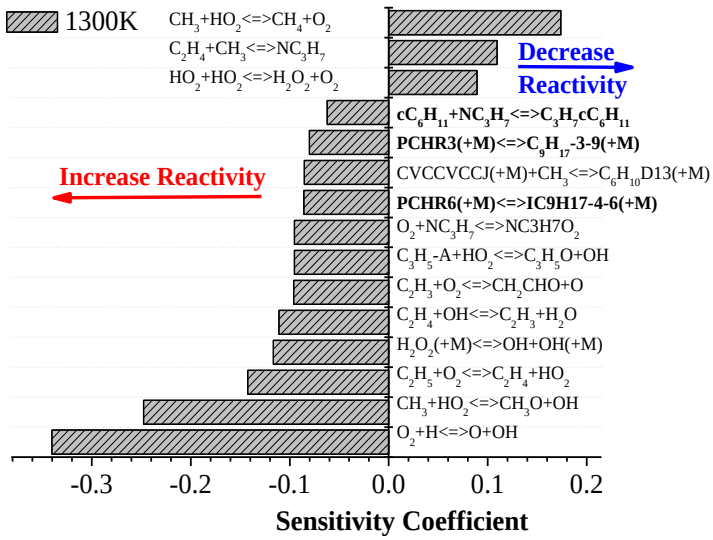

Fig. 7. “Brute force” sensitivity analyses for an ignition delay time from a fuel/air mixture at p = 10 bar, T = 1300 K, and φ = 1.0. Top fifteen reactions in the sensitivity coefficient magnitude ranking are displayed here.

3.3. H-atom abstraction from nPCH

H-atom abstraction reactions by radicals and atoms (OH, HO_2, H) are among the most important consumption channels of nPCH, which have been included in the current study. There are seven different C_9H_{17} radicals (PCHR1–PCHR7) formed by this reaction class, in which the numbers show the corresponding carbon sites. The molecular structure of nPCH with seven different carbon sites defined from 1 to 7, as presented in the Fig. 8.

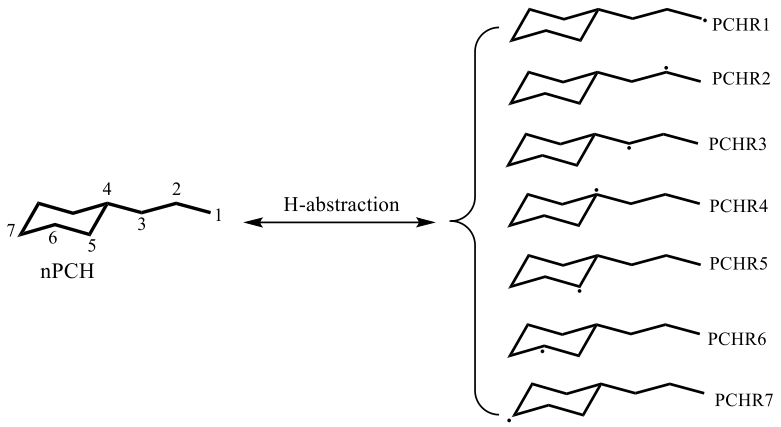

Fig. 8. H-atom abstraction reactions from nPCH by different radicals or atoms.

3.3.1. H-atom abstraction by OH radical

As shown in Fig. 9 , the predicted IDTs are highly sensitive to the H-atom abstraction reactions by OH radical at a low temperature of T = 700 K and abstracting from different sites shows different effects on either promoting reactivity or inhibiting reactivity. The reaction resulting in the formation of the PCHR7 radical lowers reactivity the most. Because at low temperatures molecular oxygen adds to PCHR7 radial forming PCHR7OO radical easily. Due to the influence of steric hindrance and symmetry of ring for PCHR7OO radical, the H-shift reaction of PCHR7OO radical is inhibited because the axial H and axial OO group are on the opposite sides of the ring which influences PCHR7OO radical reactivity. While the reaction of formation of the PCHR3 radical promotes reactivity the most as the subsequent reactions of the PCHR3OO radical formed via PCHR3+O_2 <=> PCHR3OO can accelerate low-temperature oxidation through chain-branching reactions.

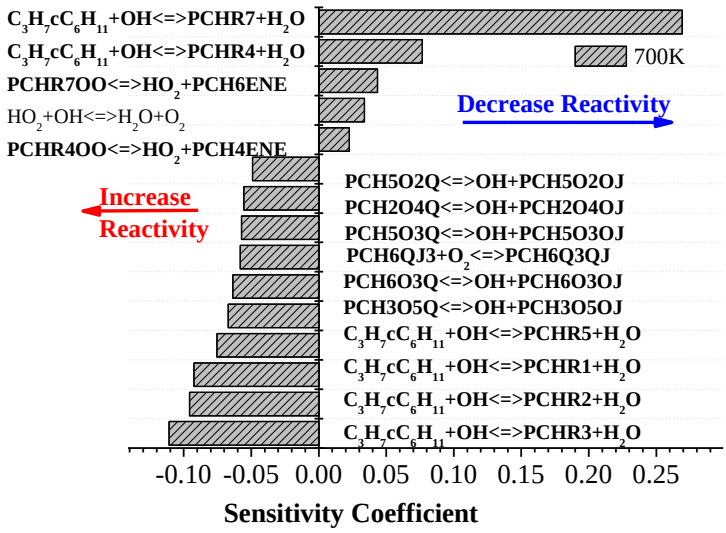

Fig. 9. “Brute force” sensitivity analyses for an ignition delay time from a fuel/air mixture at p = 10 bar, T = 700 K, and φ = 1.0. Top fifteen reactions in the sensitivity coefficient magnitude ranking

are displayed here.

Sivaramakrishnan et al. have reported the total rate constants of the reactions of the OH radical and C3–C8 alkanes [52, 53], cycloalkanes and methylcycloalkanes [54] measured using a reflected wave shock tube and computed at the G3//B3LYP//6-31G(d) level of theory combined with conventional transition state theory. In our model, the rate constants for the H-atom abstraction reactions by the OH radical on the ring sites were taken from the similar reactions of methylcycloalkane by Sivaramakrishnan et al. [54], while those on the sidechain sites were taken from similar reactions of alkanes by Sivaramakrishnan et al. [52, 53]. Considering that this treatment may introduce some uncertainties in the model because methylcyclohexane does not have a longer sidechain and alkanes do not have ring-structure, reasonable modifications of rate constants for these reactions are needed before the rate constants can be adopted. The rate constants of the H-atom abstraction by OH radical have been increased by a factor of two which is within the uncertainty of experiment and theoretical calculations. Future experimental measurements and/or theoretical calculations for these important reactions would be helpful in improving the current model.

3.3.2. H-atom abstraction by HO_2 radical

As shown in Fig. 10, with the increase of temperature up to 950 K, the reactions of H-atom abstraction from the nPCH by the HO_2 radical show high sensitivity promoting reactivity, as these reactions consume HO_2 radical to form H_2O_2, followed by its decomposition to produce two highly reactive OH radicals.

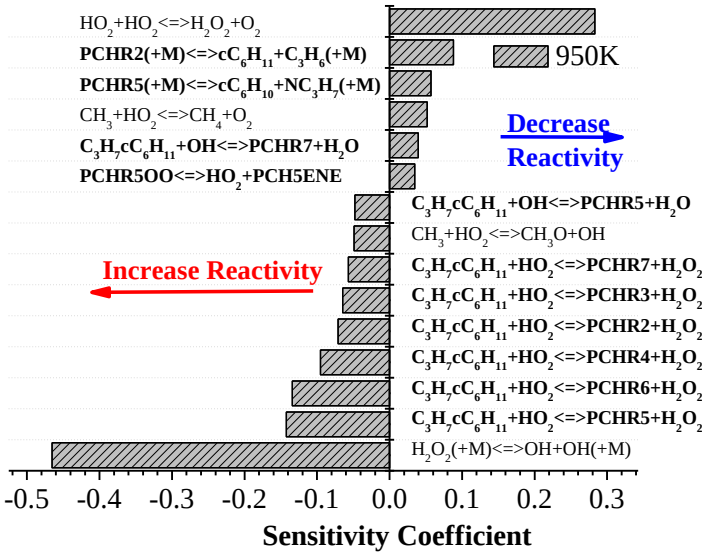

Fig. 10. “Brute force” sensitivity analyses for an ignition delay time from a fuel/air mixture at p = 10 bar, T = 950 K, and φ = 1.0. Top fifteen reactions in the sensitivity coefficient magnitude ranking are displayed here.

Carstensen et al. [55] investigated rate constants for the H-atom abstractions from alkanes by a series of ROO radicals (R = H, CH_3, C_2H_5, C_3H_7, C_4H_9, HC=O, and

$CH_3C=O$) at the CBS/QB3//B3LYP/CBSB7 level of theory systematically, and provided rate rules for primary/secondary/tertiary C–H abstractions by the HO_2 radical. Aguilera-Iparraguirre et al. [56] carried out an accurate benchmark calculation of the reaction barrier height between HO_2 radical and methane, which was used to correct those for HO_2+alkanes C_nH_{2n+2} with n = 2–4 calculated at the CCSD/cc-pVTZ level of theory. According to the carbon type, the rate constants of the reactions for H-atom abstraction from alkanes by HO_2 radical were provided. Besides, Orme et al. [57] also recommended rate rules for site-specific hydrogen atom abstraction reactions (primary, secondary, and tertiary) by the HO_2 radical. The comparison of rate constants from various resources was displayed in the SMM Fig. S1. In this work, the rate constants for these reactions were taken from the rate rules from Aguilera-Iparraguirre et al [56].

3.3.3. H-atom abstraction by H atom

Laminar flame speed sensitivity analysis results are presented in Fig. 11. The reaction of $C_3H_7cC_6H_{11}$+H <=> PCHR4+H_2 is the only highlighted sensitive reaction associated with the fuel's chemistry. It inhibits the overall reactivity because the consumption of the reactive hydrogen atom produces the relatively unreactive PCHR4 radical. Orme et al. [57] proposed rate rules for site-specific hydrogen atom abstraction reactions by various radicals (H, OH, CH_3, HO_2, CH_3O_2, CH_3O, O, O_2). These rate rules for H-atom abstraction reactions by H atom were used by Weber et al. [58] to develop their methylcyclohexane model. In this work, the analogous rate constants for H-atom abstraction by H atom at the primary, secondary, and tertiary sites recommended by Orme et al. [57] were used.

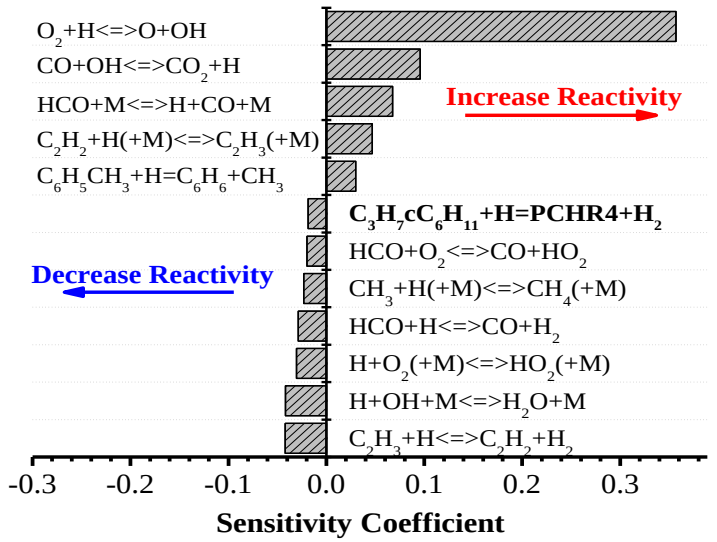

Fig. 11. Laminar flame speed sensitivity analysis for a fuel/air mixture at φ = 1.05, T = 403 K, and p = 1.01 bar. Top twelve reactions in the sensitivity coefficient magnitude ranking are displayed here.

3.4. Fuel-related radical decomposition reactions

Seven fuel-related radicals (PCHR1–PCHR7) decompose quickly to yield smaller species and cyclic compounds through the β-scission reactions (inhibiting reactivity),

or form C9 alkenyl radicals by the ring-opening reactions (promoting reactivity) which influence IDTs of nPCH at intermediate-to-high temperatures, as shown in Fig. 7 and Fig. 10.

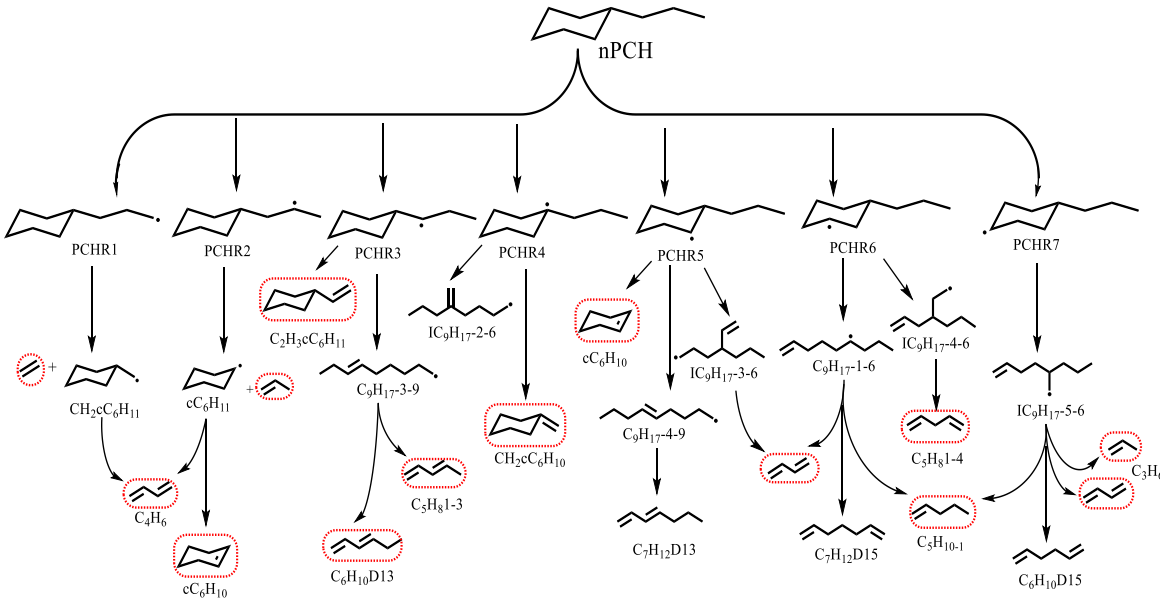

Fig. 12. Scheme of reaction pathway analysis for 7 cyclic C_9H_{17} radicals pyrolysis with important products highlighted in red.

The main oxidation and pyrolysis products, highlighted in red in Fig. 12, were detected by Ristori et al. [12] and Wang et al. [11]. The PCHR1 and PCHR2 radicals were consumed only via *β*-scission reactions through which PCHR1 can produce ethene (C_2H_4) and methyl cyclohexyl radical ($CH_2cC_6H_{11}$), while PCHR2 can produce propylene (C_3H_6) and cyclohexyl radical (cC_6H_{11}). The reaction of PCHR2 (+M) <=> cC_6H_{11}+C_3H_6 (+M) inhibits reactivity (Fig. 10), due to the formation of a cC_6H_{11} radical which subsequently contributes to the formation of stable products such as cyclohexene, 1,3-cyclohexadiene, 1,4-cyclohexadiene, and 1,3-butadiene (C_4H_6), and finally forming benzene by the dehydrogenation reaction. PCHR3 can be consumed by two reaction pathways which can form CH_3 and vinyl-cyclohexane ($C_2H_3cC_6H_{11}$) by the *β*-scission reaction or produce a C9 straight chain alkenyl radical (C_9H_{17}-3-9) by the ring-opening reaction. Among them, the ring-opening reaction of PCHR3 (+M) <=> C_9H_{17}-3-9 (+M) which promotes the overall reactivity is dominant (Fig. 7) because the tertiary C–C bond is easier to break.

In the PCHR4 radical, the radical site is on the tertiary carbon. It can generate C_2H_5 and methylene-cyclohexane ($CH_2cC_6H_{10}$) by the sidechain *β*-scission or form a branched C9 alkenyl radical (IC_9H_{17}-2-6) through the ring-opening. For both secondary C–C bond breaking, the sidechain *β*-scission reaction is dominant because it does not involve ring strain which may cause high reaction barrier. The PCHR5 radical can be consumed by three different pathways. Cyclohexene and n-propyl radical (NC_3H_7) are formed by the sidechain *β*-scission reaction inhibiting reactivity (Fig. 10). Due to the symmetry of ring, the C9 chain alkenyl radical (C_9H_{17}-4-9) and branched C9 alkenyl

radical (IC_9H_{17}-3-6) are formed by the ring-opening reactions. The formation of C_9H_{17}-4-9 radical dominates because the tertiary C–C bond is more likely to break than the secondary C–C bond. For PCHR6 radical, there are only two ring-opening reactions because the position of the radical site is far from the sidechain. The formation of IC_9H_{17}-4-6 radical promotes the overall reactivity (Fig. 7). These two products are the main contributors to the formation of C_4H_6, 1,4-pentadiene ($C_5H_8$1-4), and 1-pentene (C_5H_{10}-1). Since the PCHR7 radical is symmetric, there is only one ring-opening product formed. The branched C9 alkenyl radical IC_9H_{17}-5-6 is the main contributor to the production of C_4H_6, C_3H_6, and C_5H_{10}-1.

The rate constants proposed by Tsang and his co-workers [59-62] have been widely used in cycloalkanes models. The rate constant for the reaction of PCHR2 (+M) <=> cC_6H_{11} + C_3H_6 (+M) was increased by a factor of two to improve the prediction of C_3H_6 in JSR and FR experiments. Besides, Sirjean et al. [63] reported that the activation energy of the *β*-scission reaction on the cyclohexane ring to form a double bond is about 7 kcal/mol larger than that of the acyclic radical. Because the reaction of PCHR5 (+M) <=> cC_6H_{10}+NC_3H_7 (+M) has not been studied in the literature, it is not acceptable to directly increase the energy barrier for this reaction by 7 kcal/mol. Rather than changing the energy barrier, the A-factor is increased by 1.5 herein.

3.5. The first oxygen addition reactions (*R+O₂ <=> ROO*) *and subsequent reactions*

At low temperatures, nPCH first undergoes H-atom abstraction reactions by the OH radical, forming seven n-propyl cyclohexyl radicals (PCHR1–PCHR7) which in turn react with oxygen to generate n-propyl cyclohexyl peroxy radicals (PCHROO), as shown in Fig. 13. The most stable structure for n-propylcyclohexane chosen in this work is the chair conformation with the n-propyl group in equatorial position (*eq*). The *eq-eq* conformer is considered generally as the most stable conformer since the bulky groups point away from each other to avoid a steric effect. Thus, when the OO group adds to the equatorial position, the dominant 1,5-H shift reaction on the ring is inhibited because of the steric hindrance. As concluded by Yang et al. [64-67], for methyl-cyclohexyl peroxy radicals (MCHROO), the methyl group preferring to occupy the equatorial position will ‘‘force” the OO group to stay at the axial position (*ax*), thereby facilitating the 1,5-H shift reaction. Therefore, the preferred conformation of the *eq*-propyl with *ax*-OO on the ring was considered in our model, as presented in Fig. 13 (d)-(g). To the best of our knowledge, there are no experimental and theoretical works on the kinetics of the above-mentioned reactions in the literature. For the first oxygen addition reactions on PCHR1 to PCHR3 (radical sites on the sidechain) rate constants derived from rate rules for normal alkyl radicals were used [68] based on the combination of variational transition state theory and Rice-Ramsperger-Kassel-Marcus theory/Master-Equation (RRKM/ME) with potential energy surface obtained at the CASPT2(7,5)/aug-cc-pVDZ//B3LYP/6-311G(d,p) level of theory. For the PCHR4-PCHR7 radicals (radical sites on the ring), rate constants were adopted from the similar reactions of cyclohexyl radical [69, 70] at the CASPT2(7,5)/CBS level of theory combined with variable reaction coordinate transition state theory and RRKM/ME calculations. Zou et al. [71] suggested that the activation energy of the first O_2 addition

reaction of PCHR4 radical is reduced by 1 kcal/mol, considering that the PCHR4 radical has a tertiary C–H group which is more active than a secondary C–H.

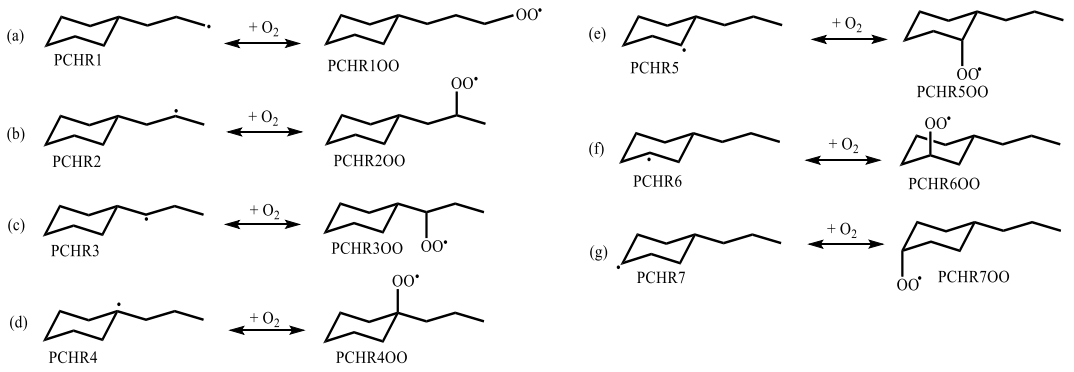

Fig. 13. The first oxygen addition reactions for PCHR radicals forming PCHROO radicals.

3.5.1. ROO radical isomerization (*ROO <=> QOOH*)

Isomerization reactions for ROO radicals play a critical role in nPCH's low-temperature oxidation. It should be noted that the conformational analysis for the isomerization reaction of alkyl cyclohexyl peroxy plays a very important role in developing the low-temperature mechanism because it dictates the possible reaction pathways and influences the product distribution. As discussed before, the preferred conformation of ROO radicals with the *eq*-propyl and *ax*-OO were considered in our model and the hydrogen atom on the axial position of the ring is easily abstracted by the axial OO group via H-shift reaction. It is worth noting that for the 1,4-H shift reaction of PCHR5OO and1,6-H shift reaction PCHR7OO radicals, when the n-propyl group is at the equatorial position, the tertiary H is only at the axial position preventing removal by the *ax*-OO group since the tertiary H and the OO group are on opposite sides of the ring plane, as shown in the SMM Fig. S2. Yao et al. [72] used the transition state theory (TST) and RRKM/ME to calculate the pressure-dependent rate constants for H-migration reactions of normal-alkyl cyclohexyl peroxy radicals at the CBS/QB3//B3LYP/CBSB7 level of theory which were adopted in our mechanism.

3.5.2 Concerted HO_2 elimination reactions from ROO (*ROO <=> Cycloalkenes+HO_2*)

The HO_2 concerted elimination reactions from ROO radicals compete with the isomerization reactions of ROO to form QOOH radicals. Previous theoretical [73] and experimental [74] studies illustrated that the direct HO_2 elimination reactions of ROO <=> alkenes+HO_2 contribute significantly to the formation of HO_2 radicals. As shown in Fig. 9 and Fig. 10, the IDTs of nPCH are sensitive to this reaction class which inhibits the overall reactivity at low-to-intermediate temperatures because ROO radicals convert to the relatively unreactive HO_2 radical and stable cycloalkenes. The rate constants for this reaction class with radical sites on the ring were estimated based on the rate constants of similar reactions for cyclohexane [69, 70] at the G2(MP2) level of theory. The rate constants of these reactions, when radical sites are on the sidechain, were taken from similar reactions of alkanes as calculated by Villano et al. [75] at the

CBS-QB3 level of theory. It should be noted that the reaction of PCHR5OO <=> HO_2+PCH4ENE is not accessible because the tertiary H is at the axial position and cannot be abstracted by the axial OO group on the adjacent carbon which is influenced by the steric hindrance, as presented in the SMM Fig. S3.

3.6. The second oxygen addition reactions (*QOOH+O_2 <=> OOQOOH*) *and subsequent reactions*

As shown in Fig. 9, the second oxygen addition reactions were identified by sensitivity analysis of IDTs at low temperatures promoting reactivity. As calculated by Yao et al. [72], the QOOH radicals produced via the 1,5- and 1,6-H shifts of ROO radicals are the most dominant products for nPCH low-temperature oxidation, followed by the second oxygen addition reactions. Since the axial hydrogen atom on the ring can be easily abstracted by the axial OO group of the ROO radicals via the H-shift reaction, the second oxygen is added to the axial position to form OOQOOH radicals with *ax*-OO, *ax*-OOH, and *eq*-propyl which are trans-conformers. Wang et al. [76] calculated the relative total energies of the four stereoisomers of hydroperoxyl-cyclohexylperoxy (*α,γ*-OOQOOH) at the CBS-QB3//B3LYP/6-311++G(d,p) level of theory, with *ax*-OOH/*ax*-OO (0 kcal mol^{-1}), *ax*-OOH/*eq*-OO (0.9 kcal mol^{-1}), *eq*-OOH/*ax*-OO (1.0 kcal mol^{-1}), and *eq*-OOH/*eq*-OO (1.5 kcal mol^{-1}) and the results show that the *ax*-OOH/*ax*-OO conformer is the most stable. This is because of the hydrogen bonding effect between the *ax*-OOH group and the *ax*-OO group. Hence, in the current model, the most stable conformer of OOQOOH radicals is that where the hydroperoxy and peroxy groups are on the axial position. Rate constants of the second oxygen addition reactions were estimated by analogy with those of the first oxygen addition reactions. Goldsmith et al. [77] concluded that the rate constants for the second oxygen addition reactions are a factor of two slower than those of the first oxygen addition reactions. Although this rate rule is used in our model, further studies for these reactions are needed to provide accurate rate constants to better understand the low-temperature chemistry for alkylcyclohexane oxidation. Except for chain branching reactions of QOOH radicals, the decomposition reactions of QOOH include QOOH <=> cyclic ether+OH, *β*-QOOH <=> cycloalkenes+HO_2, and *γ*-QOOH <=> alkene+ carbonyl or aldehyde+OH (*β*-scission products) are considered in the current model. Rate constants for these reactions on the sidechain were taken from similar reactions of alkanes [78], while rate constants for these reactions on the ring were taken from similar reactions of cyclohexane [69, 70] and methylcyclohexane [79].

There are three types for the QOOH radicals involving *β*-QOOH, *γ*-QOOH and *δ*-QOOH radicals. It should be noted that the products of the decomposition reaction of *γ*-QOOH radicals depend on the position of radical site, e.g., PCH4QJ6 and PCH4QJ2 radicals in Fig. 14. PCH4QJ6 radical yields 4-member ring bicyclic ether (PCHYO46) and OH radical through the cyclization reaction, or forms nonenone and OH radical through the direct *β*-ring-opening reaction, while PCH4QJ2 yields another 4-member ring bicyclic ether (PCHYO24) and OH radical through the cyclization reaction, or produces C_3H_6, cyclohexanone, and OH radical through the *β*-scission reaction. Walker and Morley [80] concluded that the 4-membered ring bicyclic ether is very unstable and

decomposes very quickly to form 1-hexenal. Hence, the 4-membered ring bicyclic ether PCHYO46 in Fig. 14 (a) was treated as kinetically insignificant species and is not considered in the kinetic model. For the other 4-membered ring bicyclic ether PCHYO24 in Fig. 14 (b), the four-membered cyclic ether lies on the sidechain in which only the four membered cyclic ether involves ring-opening reaction to yield either cyclohexanone and propene, or methylenecyclohexane and acetaldehyde. However, the formed bicyclic ethers from β-QOOH and δ-QOOH radicals are stable and their chemistry were included in the model.

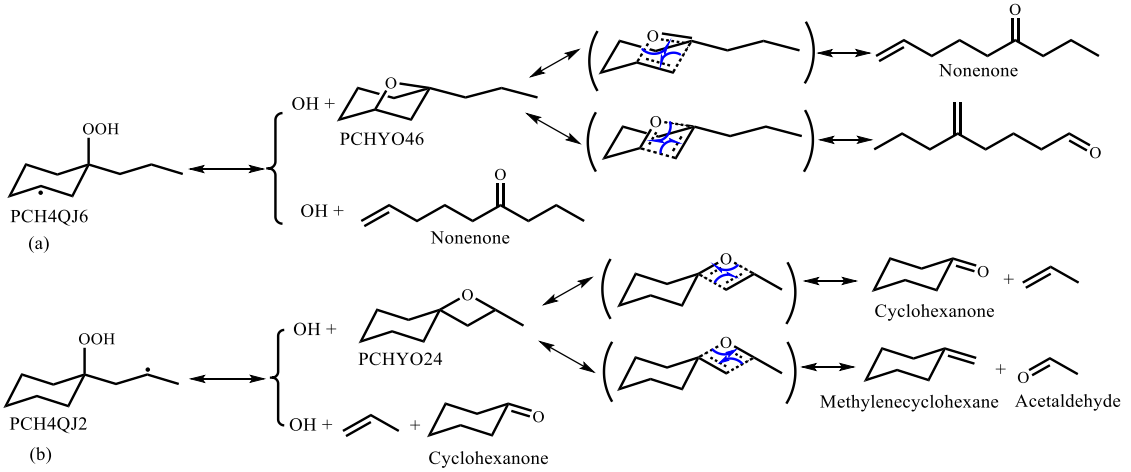

Fig. 14. Different decomposition products from the decomposition of γ-QOOH radicals.

3.6.1. OOQOOH radical isomerization (*OOQOOH <=> HOOPOOH*)

The conformational analysis of OOQOOH radicals is discussed in Section 3.6. The OOQOOH radicals with *ax*-OO, *ax*-OOH, and *eq*-propyl were found to be the most stable conformers and the 1,5-H shift reactions for the seven OOQOOH radicals with both axial OO and OOH groups on the ring need to be treated carefully since the equatorial hydrogen atom cannot be abstracted by the axial OO group, as shown in Fig. 15. Rate constants for the OOQOOH radical isomerization reactions were adopted by analogy with those of the ROO radical isomerization reactions calculated by Yao et al. [72] with the consideration of degeneracy. However, this treatment can introduce some uncertainties for model prediction because the hydrogen bond between the OOH and OO groups may influence rate constants. Further studies on rate constants for this reaction class are needed.

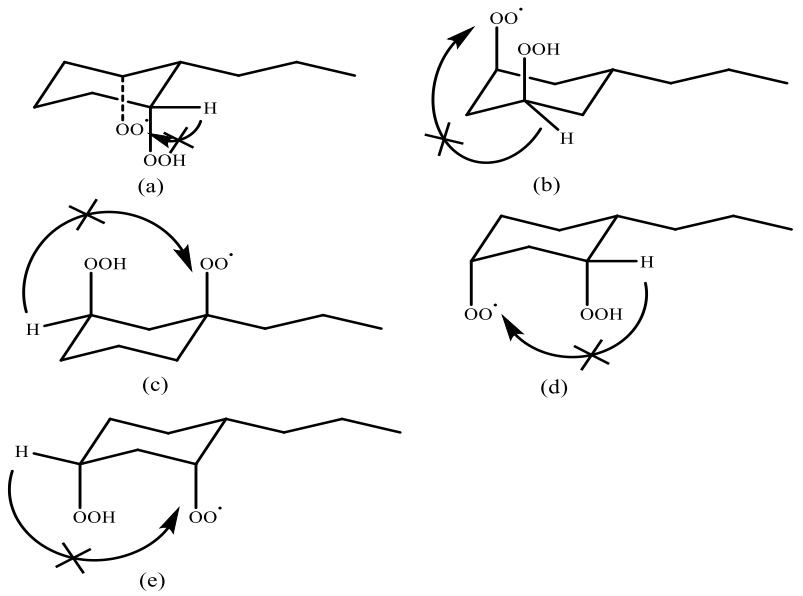

Fig. 15. Inhibited 1,5-H shift reactions for OOQOOH radicals.

H-atom on the carbon atom bonded to the OOH group can be removed easily by the OO group to yield unstable hydroperoxyalkyl peroxy products (HOOPOOH), which will decompose very quickly to produce ketohydroperoxy (KHP) and OH radical. Therefore, the current mechanism considers that OOQOOH radicals isomerize directly to form KHP and OH. These reactions are sensitive to nPCH ignition and promote the overall reactivity as highlighted in Fig. 7. Rate constants for the reactions of OOQOOH <=> KHP+OH were assigned using the same rate constants as those of the isomerization reactions (ROO <=> QOOH) with some reasonable adjustments, including that the isomerization reactions were considered to occur only on the sidechain (Fig. 16 (a)) or happen between sidechain and ring (Fig. 16 (b)), that the activation energies of these reactions were reduced by 3 kcal/mol, and that the preexponential factor was adjusted with the consideration of degeneracy. For the isomerization reactions that only happen on the ring (Fig. 16 (c)), Bissoonauth et al. [81] suggested that the activation energies of these reactions were reduced by 2 kcal/mol rather than 3 kcal/mol with the consideration of the potential ring strain, and the preexponential factor should also be adjusted with the consideration of degeneracy.

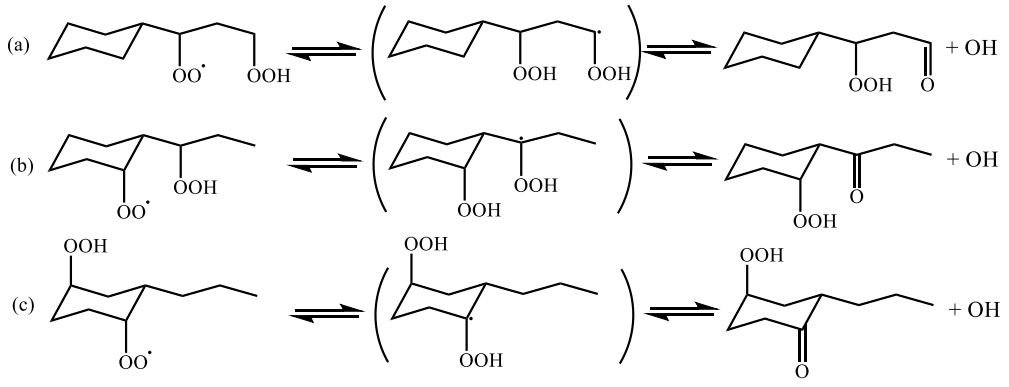

Fig. 16. Pathways of OOQOOH radials to form cyclic ketohydroperoxy (KHP) and OH radical.

4. Model validation

The developed mechanism herein is validated comprehensively against different experimental datasets from this work and literature data including IDTs (Fig. 17 and SMM Figs. S4-S5), speciation results from a JSR and a FR (Fig. 20, Fig. 21, and the SMM Figs. S6-S16, and laminar flame speeds (Fig. 22).

4.1. Ignition delay time validation

IDT measurements carried out in the current work using a HPST and an RCM and covering T = 615–1400 K, p = 10–40 bar, and φ = 0.5–2.0 are presented here, together with the predictions from the current model. Besides, our model is also validated against the HPST (Fig. 17) and RCM (SMM Fig. S4) experimental results from Ahmed et al. [6], and ST (SMM Fig. S5) experimental results from Dubois et al. [5]. It is of interest to note from our RCM experiments that a distinct three-stage ignition phenomenon was observed at φ = 0.25. The underlying chemistry and characteristics (temperature, pressure, heat release rate, key species concentration, and heat production per reaction) of nPCH multi-stage ignition is discussed in detail in a companion study [82]. Moreover, the present model can capture well the newly-acquired IDT data from this work and the literature [6] over a wide range of temperatures, pressures, and equivalence ratios and is also in good agreement with the measured multi-stage IDTs.

Fig. 17 shows the influence of pressure on IDTs of nPCH/air mixtures in HPST and RCM at φ = 0.5, 1.0, and 2.0. When the pressure increases, the experimental results show shortened IDTs at all equivalence ratios investigated, which can be explained by the increasing concentrations of the reactants that enhance the overall reactivity. Besides, Fig. 17 shows the effect of equivalence ratio on IDTs of nPCH/air mixtures at p = 10–40 bar. At low temperatures, the increasing of nPCH concentration contributes to the increasing concentrations of species involved in the low-temperature oxidation sequence. This is a chain-branching process since nPCH consumes a OH radical and produces two OH radicals and one carbonyl-alkoxy OP=O, thereby accelerating nPCH low-temperature oxidation. However, at high temperatures, the differences between IDTs obtained under different equivalence ratios become small. This is because the high-temperature chemistry is controlled mainly by the C0–C2 core mechanism, especially the reaction of H+O_2 <=> O+OH is important in accelerating nPCH high-temperature oxidation. Comparing the literature HPST IDT data with the RCM data obtained in this work, it is seen that the HPST and RCM data complement each other well, with the former and the latter covering intermediate-to-high temperatures and low-to-intermediate temperatures, respectively. This illustrates the significance of the new RCM data acquired in the current study by extending the model validation condition range to low temperatures. Examining the combined HPST and RCM data as a whole, a clear slope change is noted at around 760–1000 K on the Arrhenius plots shown in Fig. 17. This suggests that nPCH exhibits NTC response at a wide range of conditions, which has been successfully captured by the current model. The NTC response of nPCH can be attributed to the reverse reactions of R+O_2 <=> ROO and the HO_2 concerted

elimination reactions of ROO radicals. Meanwhile, the QOOH radicals tend to form either cyclic ether and OH radical, cycloalkene and HO_2 radical, and β-scission products, as shown in Fig. 5 in black. This process is different from the low-temperature chain-branching reaction pathway as there is only one radical formed rather than three radicals, resulting in the increase of IDT with the increasing of temperature.

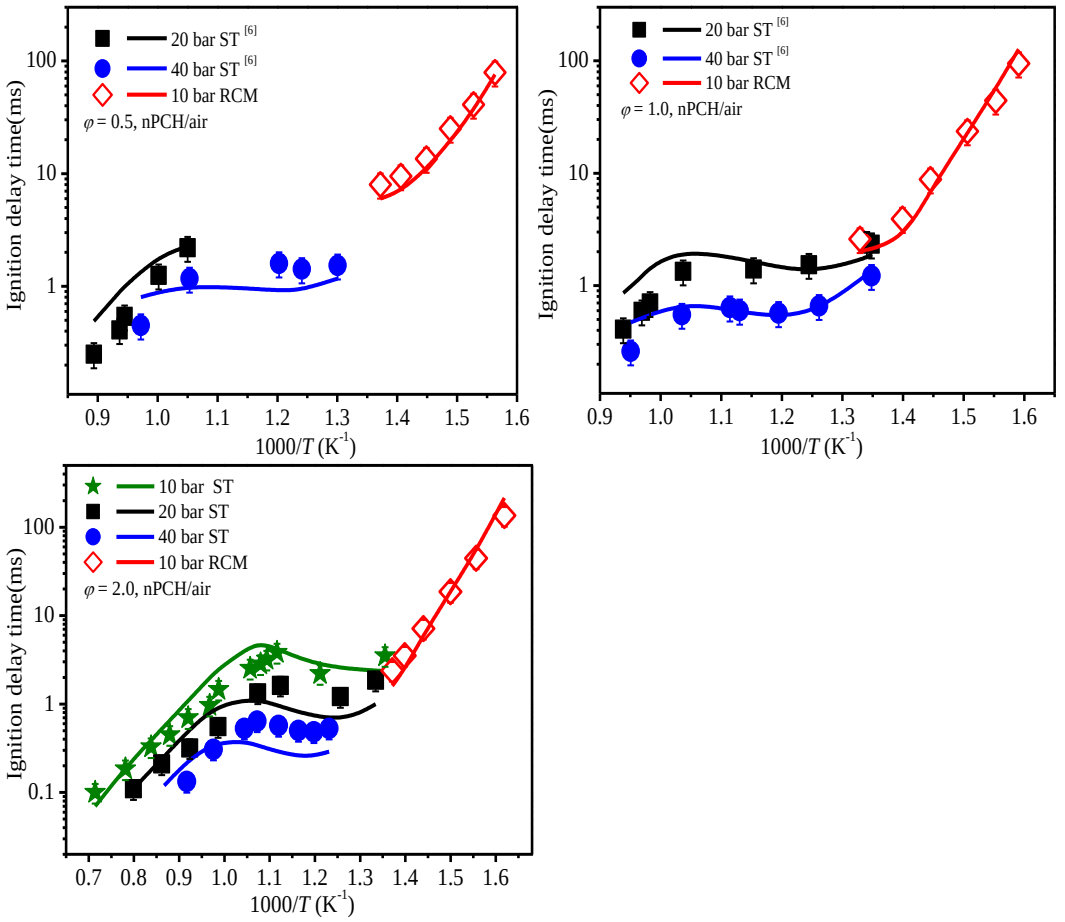

Fig. 17. Comparison of nPCH/air ignition delay times predicted from the current model, measured in the HPST and an RCM experiments of this work, and reported HPST data of [6]. Solid symbols: shock tube data; open symbols: RCM data; solid lines: the current model predictions.

4.2. Flux analyses

Flux analyses were carried out at the same conditions as those for sensitivity analyses, i.e., at T = 700 K, 950 K, and 1300 K, φ = 1.0 and p = 10 bar. As shown in Fig. 18, at low temperature of T = 700 K, nPCH is consumed by H-atom abstraction reactions by OH radical to form seven n-propyl cyclohexyl (PCHR1–PCHR7) radicals. Subsequently, more than 80% of PCHR1–PCHR7 radicals react with oxygen yielding ROO radicals which promotes reactivity, followed by isomerization reaction. Here, we take PCH6QJ3 radical produced from PCHR6OO radical as an example in Fig. 19. 50.4% of PCHR6OO radicals are consumed through the isomerization reaction yielding the PCH6QJ3 radical. Then, the second oxygen addition reaction consumes 86.6% of the PCH6QJ3 radical to form the PCH6Q3QJ radical, promoting reactivity. This is followed by the reaction of PCH6Q3QJ <=> PCH6O3Q+OH, which accounts for 58.4%

of the PCH6Q3QJ radical consumption. Eventually, the PCH6O3Q radical converts completely to the PCH6O3OJ radical and another OH radical.

With the temperature increasing up to 950 K, the H-atom abstraction reactions from nPCH by the HO_2 radical become increasingly important in promoting oxidation. Moreover, the first oxygen addition reactions on PCHR radicals are competitive with the isomerization and decomposition reactions of those radicals. For example, the isomerization reaction PCHR6 <=> PCHR2 accounts for 26.6% of the PCHR6 radical consumption at 950 K, while this pathway is not important at 700 K. In addition, the decomposition reactions PCHR2 (+M) <=> cC_6H_{11}+C_3H_6 (+M) and PCHR5 (+M) <=> cC_6H_{10}+NC_3H_7 (+M) become increasingly important in inhibiting reactivity; they accounted for 44.5% of PCHR2 consumption and 25.4% of PCHR5 consumption, respectively. These β-scission products will produce stable cyclic species, e.g., benzene, which can lead to soot formation.

At temperatures above 1300 K, the reaction of $C_3H_7cC_6H_{11}$+H <=> PCHR4+H_2 is highlighted in laminar flame speed sensitivity analysis where it inhibits reactivity with a contribution of 4.2% to nPCH consumption. Besides, the unimolecular decomposition cC_6H_{11}+NC_3H_7 <=> $C_3H_7cC_6H_{11}$ promotes the overall reactivity at high-temperature (1300 K), as indicated by IDT sensitivity analysis; it contributes to 1.6% of nPCH consumption. For the PCHR1–PCHR7 radicals, their decomposition reactions involving ring-opening become increasingly important. For example, the reactions of PCHR3 (+M) <=> C_9H_{17}-3-9 (+M) and PCHR6 (+M) <=> IC_9H_{17}-4-6 (+M) which promote reactivity accounting for 61.6% of the PCHR3 radical consumption and for 28.0% of the PCHR6 radical consumption, respectively. The C9 alkenyl radicals will decompose to yield small species and radicals, thereby accelerating nPCH consumption. Compared with their β-scission reaction, it is found that the ring-opening reaction, involving ring strain and causing high reaction barrier, proceeds at higher temperature.

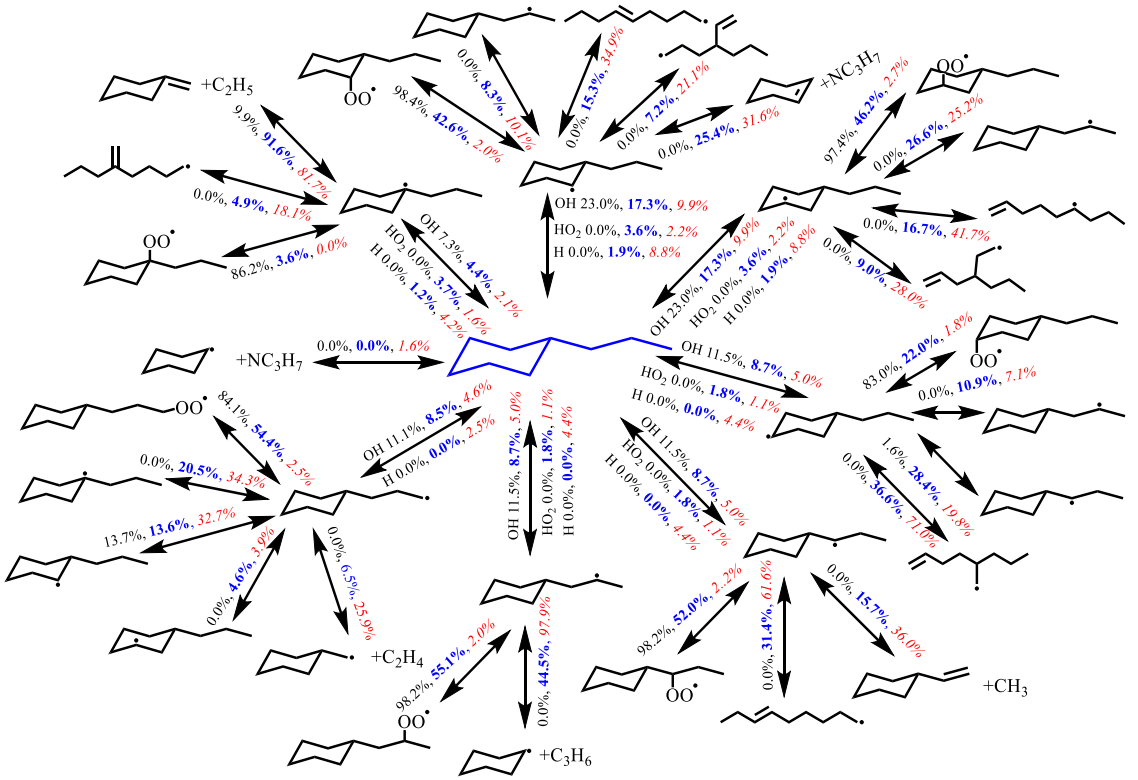

Fig. 18. Flux analysis for the oxidation of stoichiometric nPCH/air at p = 10 bar, T = 700 K (black), 950 K (blue and bold) and 1300 K (red and italics), and 20% fuel consumption assuming a constant volume reactor.

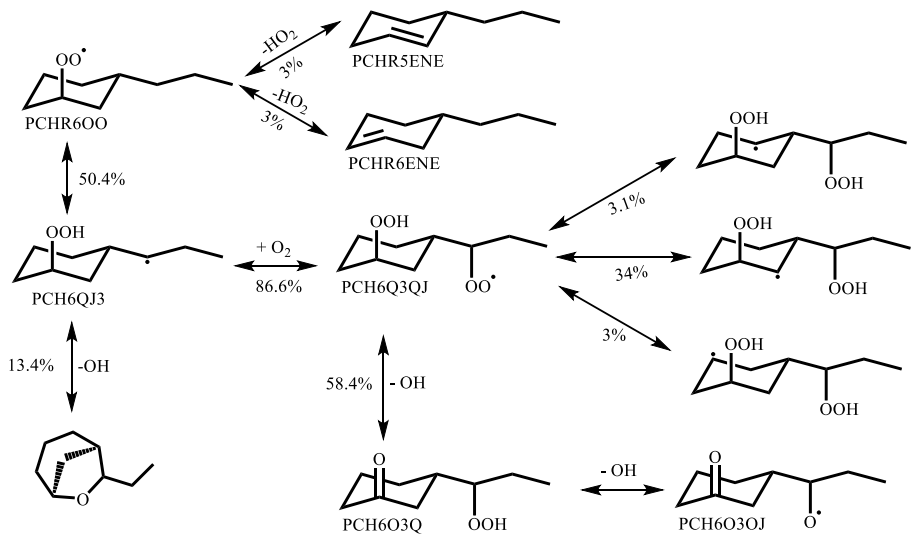

Fig. 19. Flux analysis of PCH6QJ3 radical produced from PCHR6OO for the oxidation of stoichiometric nPCH/air at p = 10 bar, T = 700 K and 20% fuel consumption assuming a constant volume reactor.

4.3. Species validations

4.3.1. Jet-stirred reactor results

Ristori et al. [12] measured the concentration profiles of stable species over a temperature range of 950–1250 K during the oxidation of highly diluted nPCH/O_2/N_2 mixtures in a jet-stirred reactor at atmospheric pressure and equivalence ratios of 0.5–1.5. Here, we present the simulation results from the current model against the experimental data at φ = 1.5, while the results for φ = 0.5 and 1.0 are shown in Figs. S6–S7 in SMM. There is good agreement between the model predictions and experimental measurements, as shown in Fig. 20. The concentrations of H_2, O_2, CO, and CO_2 are the highest among all measured species. Besides, the concentrations of CH_4, C_2H_2, C_2H_4, C_3H_6, and C_4H_6 are the second highest. Among them, C_2H_4, C_3H_6, and C_4H_6 can be produced through the decomposition reactions of seven n-propyl cyclohexyl radicals. These decomposition reactions also contribute significantly to the formation of the above mentioned C5 species, as discussed in Section 3.4. However, it is seen from Fig. 20 that the concentrations of 1,3-pentadiene and benzene are underestimated in the simulations. To improve prediction of these intermediate C5–C8 species, the rate constants for the reactions involving these species need to be further investigated and updated.

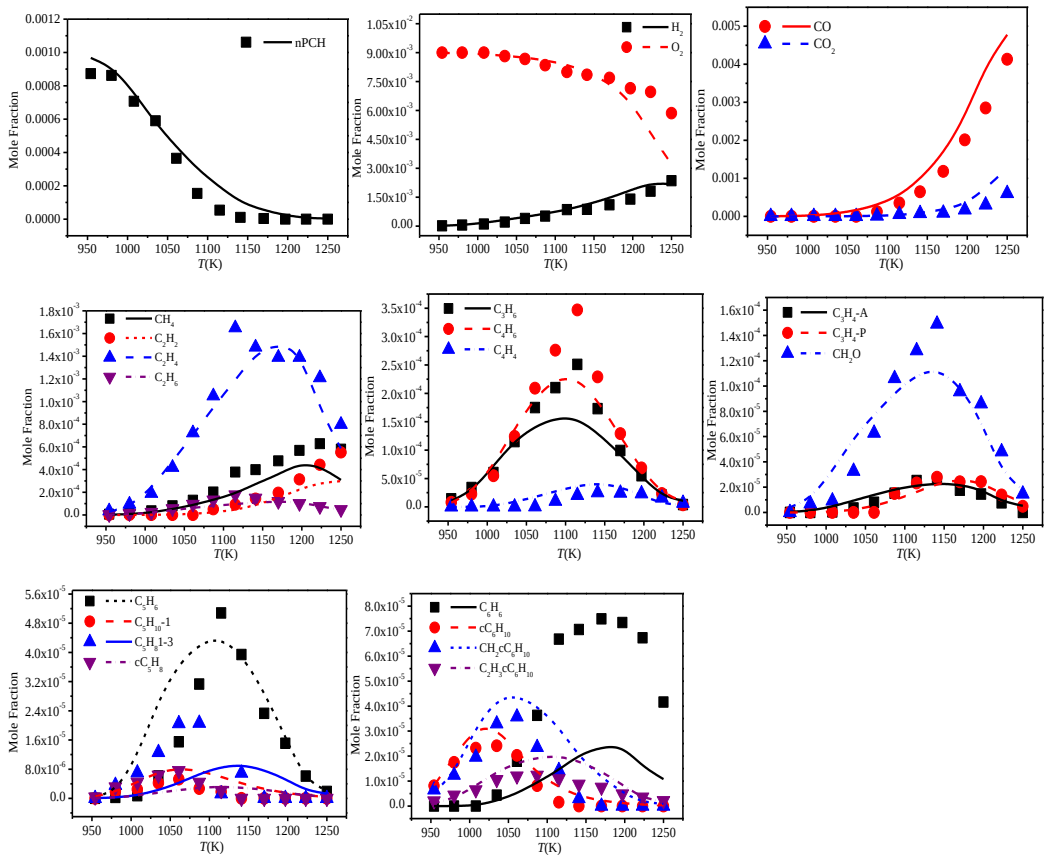

Fig. 20. Speciation result comparison for the conditions of 0.1% nPCH, 0.9% O_2, 99% N_2, φ = 1.5, p = 1.01 bar, and residence time of 0.07 s. Symbols: JSR experimental measurements [12]; solid lines: the current model predictions.

4.3.2. Flow reactor results

Wang et al. [11] conducted nPCH pyrolysis experiments in a flow reactor combined

with a mass spectrometry detection system in the temperature range of 950–1300 K at pressures of 0.04 and 1 bar with an initial mole concentration of nPCH being 0.5%. Fig. 21 compares the model predictions against the experimental results of [11] at p = 1 bar. The comparative results at p = 0.04 bar are shown in Fig. S16 in SMM. The concentrations of C_2H_4, C_3H_6, and C_4H_6 are the highest among the pyrolytic products. Besides, the concentrations of cyclohexene (cC_6H_{10}), benzene (C_6H_6), and 1,3-pentadiene (C_5H_8-13) are relatively high. These species are mainly formed via the decomposition of the seven cyclic C_9H_{17} radicals. The current model can capture these measured mole fraction profiles well, especially aromatic species, including C_6H_6, fulvene, toluene, phenylacetylene, styrene, and ethylbenzene which are thought to be the inception sites for soot growth. Accurate predictions of these species can help understand their formation and destruction pathways, which are important for controlling pollutant formation.

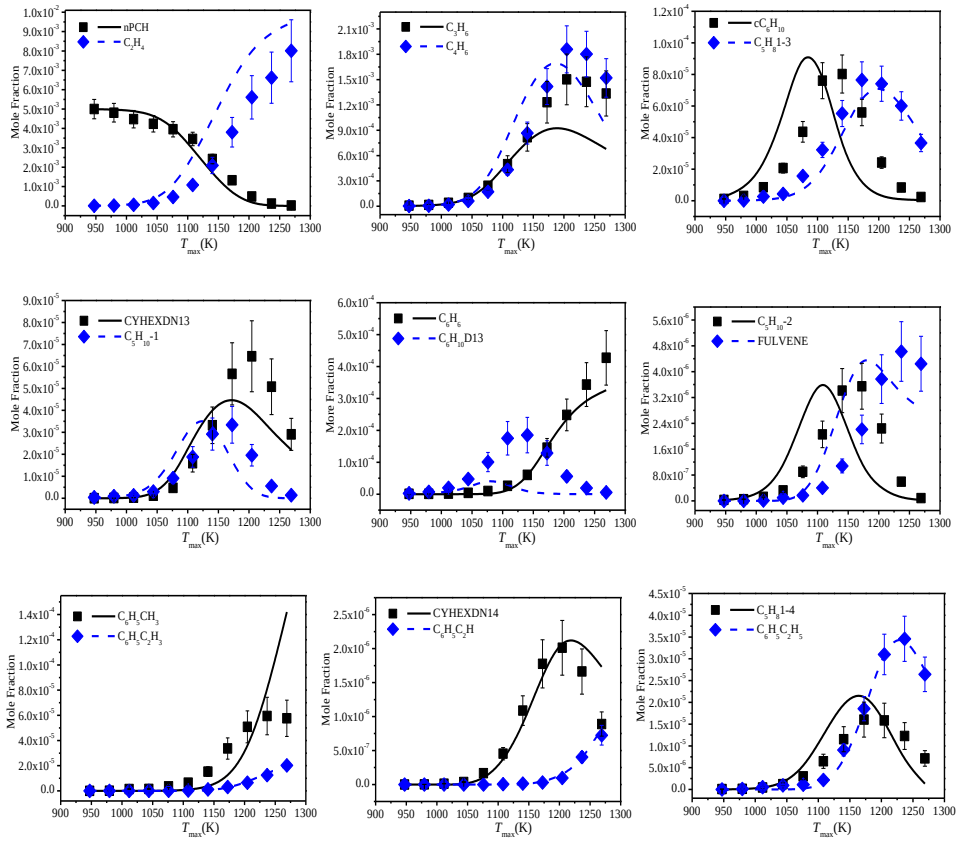

Fig. 21. Speciation result comparison for the conditions of 0.5% nPCH in He and p = 1 bar, Symbols: FR experimental measurements [11]; Lines: the current model predictions.

4.4. Laminar flame speed validations

Laminar flame speeds for nPCH in air carried out in the current work from TAMU are presented here at p = 1.01 and 3.04 bar, T = 403 K, and φ = 0.7–1.4. Dubois et al. [5] and Ji et al. [9] also measured the laminar flame speeds for nPCH in air at atmosphere pressure at preheat temperatures of 403 K and 353 K, respectively. The peak in both laminar flame speed experiments occur at $\varphi \sim 1.05$. The predictions of the current model are in good agreement with the experimental results from this work and

literature, and capture the locations of peak laminar flame speed well, as shown in Fig. 22.

Laminar flame speed sensitivity analysis was also performed at φ = 1.05, 403 K preheat, and p = 1.01 bar, as shown in Fig. 11. Most of significant reactions highlighted there are from the C0–C2 sub-mechanism. The chain branching reaction of O_2+H <=> O+OH is the most sensitive reaction for laminar flame speed predictions. The only sensitive fuel-related reaction identified is $C_3H_7cC_6H_{11}$+H <=> PCHR$_4$+H_2, but its sensitivity coefficient is small in comparison to the others. This reaction contributes a little for laminar flame speed, as altering its rate constant has very limited effect on the predictions.

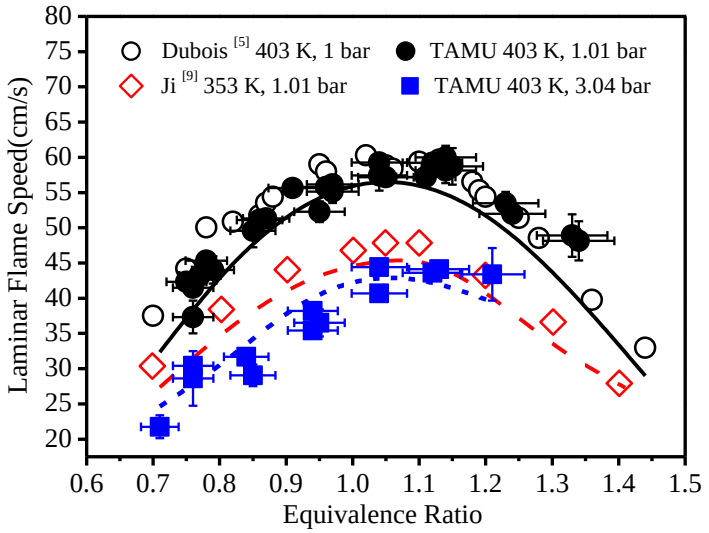

Fig. 22. Laminar flame speeds for nPCH/air mixtures. Solid symbols: experimental results from the current work; open symbols: experimental results of [5, 9]; Lines: the current model predictions.

5. Conclusions

A detailed chemical kinetic model covering low- to high-temperature chemistry has been developed to describe nPCH combustion, based on the combination of comprehensive core mechanism taken from AramcoMech 3.0 and 34 low- to high-temperature reaction classes. The new IDT datasets over the temperature range 615–1400 K, at pressures of 10, 20, and 40 bar, and equivalence ratios of 0.5, 1.0, and 2.0 in air were acquired using the UConn rapid compression machine and KAUST high-pressure shock tube. Additionally, laminar flame speeds were measured at an initial mixture temperature of 403 K and p = 1.01 and 3.04 bar over a range of equivalence ratios at TAMU.

The current mechanism was validated against the present experimental results and literature data well. Sensitivity analyses for IDTs and laminar flame speeds and flux analyses were carried out to identify important reactions. According to these analyses, it is found that at low temperatures, the H-atom abstraction reactions from nPCH by OH radicals control the fuel's reactivity. Then, the first and second oxygen addition reactions and their subsequent reactions are chain-branching processes which consume one OH radical and generate three radicals, thereby enhancing nPCH reactivity. At

intermediate temperatures, the importance of the H-atom abstraction reactions from nPCH by HO_2 radicals is increasing, and these reactions promote the overall reactivity. Besides, n-propyl cyclohexyl radicals (PCHR1–PCHR5) decompose to yield cyclic compounds through the β-scission reactions inhibiting reactivity. With increasing temperature, H-atom abstraction from nPCH by H atom gets more important inhibiting nPCH reactivity, as highlighted by laminar flame speed sensitivity analysis. Additionally, n-propyl cyclohexyl radicals (PCHR3–PCHR7) decompose to yield C9 alkenyl radicals through the ring-opening reactions promoting reactivity. Further experimental and theoretical studies for these important reaction classes are needed to improve the prediction of our model and better understanding of the low- to high-temperature chemistry of n-propylcyclohexane.

Declaration of Competing Interest

None

Acknowledgments

The work at Beihang University was supported by National Science and Technology Major Project (2017-III0004-0028), Sinopec Science and Technology Department, and the High-performance Computing (HPC) center of Beihang University.

References

[1] E.J. Silke, W.J. Pitz, C.K. Westbrook, M. Ribaucour, Detailed chemical kinetic modeling of cyclohexane oxidation, J. Phys. Chem. A 111 (2007) 3761-3775.

[2] W.J. Pitz, J. Liang, G. Kukkadapu, K. Zhang, C. Conroy, J. Bugler, H.J. Curran, A detailed chemical kinetic modeling and experimental investigation of the low- and high-temperature chemistry of n-butylcyclohexane, Int. J. Chem. Kinet. 53 (2020) 465-475.

[3] M.E. Law, P.R. Westmoreland, T.A. Cool, J. Wang, N. Hansen, C.A. Taatjes, T. Kasper, Benzene precursors and formation routes in a stoichiometric cyclohexane flame, Proc. Combust. Inst. 31 (2007) 565-573.

[4] P. Dagaut, A. El Bakali, A. Ristori, The combustion of kerosene: Experimental results and kinetic modelling using 1- to 3-component surrogate model fuels, Fuel 85 (2006) 944-956.

[5] T. Dubois, N. Chaumeix, C.E. Paillard, Experimental and modeling study of n-propylcyclohexane oxidation under engine-relevant conditions, Energy Fuels 23 (2009) 2453-2466.

[6] A. Ahmed, J.A. Corrubia, M. Al-Lehaibi, F. Farid, H. Wang, Z. Wang, B. Chen, W.L. Roberts, D.L. Miller, A. Farooq, N.P. Cernansky, S.M. Sarathy, A comprehensive combustion chemistry study of n-propylcyclohexane, Combust. Flame 233 (2021) 111576.

[7] Z. Tian, Y. Zhang, F. Yang, L. Pan, X. Jiang, Z. Huang, Comparative study of experimental and modeling autoignition of cyclohexane, ethylcyclohexane, and n-propylcyclohexane, Energy Fuels 28 (2014) 7159-7167.

[8] M. Crochet, R. Minetti, M. Ribaucour, G. Vanhove, A detailed experimental study of n-propylcyclohexane autoignition in lean conditions, Combust. Flame 157 (2010) 2078-2085.

[9] C. Ji, E. Dames, B. Sirjean, H. Wang, F.N. Egolfopoulos, An experimental and modeling study of the propagation of cyclohexane and mono-alkylated cyclohexane flames, Proc. Combust. Inst. 33 (2011)

971-978.
[10] N. Liu, C. Ji, F.N. Egolfopoulos, Ignition of non-premixed cyclohexane and mono-alkylated cyclohexane flames, Proc. Combust. Inst. 34 (2013) 873-880.
[11] Q. Wang, C. Wang, Y. Huang, M. Ding, J. Wang, J. Yang, Pyrolysis chemistry of n-propylcyclohexane via experimental and modeling approaches, Fuel 283 (2021) 118847.
[12] A. Ristori, P. Dagaut, A.E. Bakali, M. Cathonnet, The oxidation of n-propylcyclohexane: Experimental results and kinetic modeling, Combust. Sci. Technol. 165 (2001) 197-228.
[13] K. Mati, Ph. D. Thesis of the University of Orléans, 2005.
[14] P. Diévart, Ph. D. Thesis of the University of Orléans, 2008.
[15] E. Pousse, R. Porter, V. Warth, P.A. Glaude, R. Fournet, F. Battin-Leclerc, Lean methane premixed laminar flames doped by components of diesel fuel II: n-Propylcyclohexane, Combust. Flame 157 (2010) 75-90.
[16] J. Guo, J. Wang, X. Hua, Z. Li, N. Tan, X. Li, Mechanism construction and simulation for high-temperature combustion of n-propylcyclohexane, Chem. Res. Chin. Univ. 30 (2014) 480-488.
[17] H. Wang, E. Dames, B. Sirjean, D.A. Sheen, R. Tango, A. Violi, J.Y.W. Lai, F.N. Egolfopoulos, D.F. Davidson, R.K. Hanson, C.T. Bowman, C.K. Law, W. Tsang, N.P. Cernansky, D.L. Miller, R.P. Lindstedt, A high-temperature chemical kinetic model of n-alkane (up to n-dodecane), cyclohexane, and methyl-, ethyl-, n-propyl and n-butyl-cyclohexane oxidation at high temperatures, JetSurF version 2.0, http://web.stanford.edu/group/haiwanglab/JetSurF/JetSurF2.0/index.html.
[18] G. Mittal, C.-J. Sung, A rapid compression machine for chemical kinetics studies at elevated pressures and temperatures, Combust. Sci. Technol. 179 (2007) 497-530.
[19] A.K. Das, C.-J. Sung, Y. Zhang, G. Mittal, Ignition delay study of moist hydrogen/oxidizer mixtures using a rapid compression machine, Int. J. Hydrogen Energy 37 (2012) 6901-6911.
[20] D. Lee, S. Hochgreb, Rapid compression machines: Heat transfer and suppression of corner vortex, Combust. Flame 114 (1998) 531-545.
[21] B.W. Weber, C.J. Sung, UConnRCMPy: Python-based data analysis for rapid compression machines, 10th U.S. National Combustion Meeting (2017), paper 2D19.
[22] E.E. Dames, A.S. Rosen, B.W. Weber, C.W. Gao, C.-J. Sung, W.H. Green, A detailed combined experimental and theoretical study on dimethyl ether/propane blended oxidation, Combust. Flame 168 (2016) 310-330.
[23] R.Z. Fang, G. Kukkadapu, M.Y. Wang, S.W. Wagnon, K.W. Zhang, M. Mehl, C.K. Westbrook, W.J. Pitz, C.J. Sung, Fuel molecular structure effect on autoignition of highly branched iso-alkanes at low-to-intermediate temperatures: Iso-octane versus iso-dodecane, Combust. Flame 214 (2020) 152-166.
[24] M.C. Krejci, O. Mathieu, A.J. Vissotski, S. Ravi, T.G. Sikes, E.L. Petersen, A. Kérmonès, W. Metcalfe, H.J. Curran, Laminar Flame Speed and Ignition Delay Time Data for the Kinetic Modeling of Hydrogen and Syngas Fuel Blends, J. Eng. Gas Turb. Power 135 (2013) 0215031-0215039.
[25] Z. Chen, On the extraction of laminar flame speed and Markstein length from outwardly propagating spherical flames, Combust. Flame 158 (2011) 291-300.
[26] A.F. Forziati, F.D. Rossini, Physical properties of sixty API-NBS hydrocarbons, J. Res. Natl. Bur. Stand 43 (1949) 473-476.
[27] M. Ribaucour, R. Minetti, L.R. Sochet, H.J. Curran, W.J. Pitz, C.K. Westbrook, Ignition of isomers of pentane: An experimental and kinetic modeling study, Proc. Combust. Inst. 28 (2000) 1671-1678.
[28] C.K. Westbrook, W.J. Pitz, J.E. Boercker, H.J. Curran, J.F. Griffiths, C. Mohamed, M. Ribaucour, Detailed chemical kinetic reaction mechanisms for autoignition of isomers of heptane under rapid

compression, Proc. Combust. Inst. 29 (2002) 1311-1318.
[29] S. Tanaka, F. Ayala, J.C. Keck, A reduced chemical kinetic model for HCCI combustion of primary reference fuels in a rapid compression machine, Combust. Flame 133 (2003) 467-481.
[30] A. Kéromnès, W.K. Metcalfe, K.A. Heufer, N. Donohoe, A.K. Das, C.-J. Sung, J. Herzler, C. Naumann, P. Griebel, O. Mathieu, M.C. Krejci, E.L. Petersen, W.J. Pitz, H.J. Curran, An experimental and detailed chemical kinetic modeling study of hydrogen and syngas mixture oxidation at elevated pressures, Combust. Flame 160 (2013) 995-1011.
[31] W.K. Metcalfe, S.M. Burke, S.S. Ahmed, H.J. Curran, A hierarchical and comparative kinetic modeling study of C1−C2 hydrocarbon and oxygenated fuels, Int. J. Chem. Kinet. 45 (2013) 638-675.
[32] S.M. Burke, W. Metcalfe, O. Herbinet, F. Battin-Leclerc, F.M. Haas, J. Santner, F.L. Dryer, H.J. Curran, An experimental and modeling study of propene oxidation. Part 1: Speciation measurements in jet-stirred and flow reactors, Combust. Flame 161 (2014) 2765-2784.
[33] S.M. Burke, U. Burke, R. Mc Donagh, O. Mathieu, I. Osorio, C. Keesee, A. Morones, E.L. Petersen, W. Wang, T.A. DeVerter, M.A. Oehlschlaeger, B. Rhodes, R.K. Hanson, D.F. Davidson, B.W. Weber, C.-J. Sung, J. Santner, Y. Ju, F.M. Haas, F.L. Dryer, E.N. Volkov, E.J.K. Nilsson, A.A. Konnov, M. Alrefae, F. Khaled, A. Farooq, P. Dirrenberger, P.-A. Glaude, F. Battin-Leclerc, H.J. Curran, An experimental and modeling study of propene oxidation. Part 2: Ignition delay time and flame speed measurements, Combust. Flame 162 (2015) 296-314.
[34] C.-W. Zhou, Y. Li, E. O'Connor, K.P. Somers, S. Thion, C. Keesee, O. Mathieu, E.L. Petersen, T.A. DeVerter, M.A. Oehlschlaeger, G. Kukkadapu, C.-J. Sung, M. Alrefae, F. Khaled, A. Farooq, P. Dirrenberger, P.-A. Glaude, F. Battin-Leclerc, J. Santner, Y. Ju, T. Held, F.M. Haas, F.L. Dryer, H.J. Curran, A comprehensive experimental and modeling study of isobutene oxidation, Combust. Flame 167 (2016) 353-379.
[35] Y. Li, C.-W. Zhou, K.P. Somers, K. Zhang, H.J. Curran, The oxidation of 2-butene: A high pressure ignition delay, kinetic modeling study and reactivity comparison with isobutene and 1-butene, Proc. Combust. Inst. 36 (2017) 403-411.
[36] U. Burke, W.K. Metcalfe, S.M. Burke, K.A. Heufer, P. Dagaut, H.J. Curran, A detailed chemical kinetic modeling, ignition delay time and jet-stirred reactor study of methanol oxidation, Combust. Flame 165 (2016) 125-136.
[37] C.-W. Zhou, Y. Li, U. Burke, C. Banyon, K.P. Somers, S. Ding, S. Khan, J.W. Hargis, T. Sikes, O. Mathieu, E.L. Petersen, M. AlAbbad, A. Farooq, Y. Pan, Y. Zhang, Z. Huang, J. Lopez, Z. Loparo, S.S. Vasu, H.J. Curran, An experimental and chemical kinetic modeling study of 1,3-butadiene combustion: Ignition delay time and laminar flame speed measurements, Combust. Flame 197 (2018) 423-438.
[38] J. Bai, C. Cavallotti, C.-W. Zhou, Theoretical kinetics analysis for ȮH radical addition to 1,3-butadiene and application to model prediction, Combust. Flame 221 (2020) 228-240.
[39] M. Liu, M. Liu, X. Yao, Z. Li, J. Wang, N. Tan, X. Li, Reactions of β-hydroxypropyl radicals with O2 on the HOC3H6OO• potential energy surfaces: A theoretical study, Combust. Flame 211 (2020) 202-217.
[40] Y. Zhu, C.-W. Zhou, Chemical kinetics study of 1,3-butadiene + HȮ2; implications for combustion modeling and simulation, Combust. Flame 221 (2020) 241-255.
[41] S.M. Sarathy, C.K. Westbrook, M. Mehl, W.J. Pitz, C. Togbe, P. Dagaut, H. Wang, M.A. Oehlschlaeger, U. Niemann, K. Seshadri, P.S. Veloo, C. Ji, F.N. Egolfopoulos, T. Lu, Comprehensive chemical kinetic modeling of the oxidation of 2-methylalkanes from C7 to C20, Combust. Flame 158 (2011) 2338-2357.

[42] S.M. Sarathy, T. Javed, F. Karsenty, A. Heufer, W. Wang, S. Park, A. Elwardany, A. Farooq, C.K. Westbrook, W.J. Pitz, M.A. Oehlschlaeger, G. Dayma, H.J. Curran, P. Dagaut, A comprehensive combustion chemistry study of 2,5-dimethylhexane, Combust. Flame 161 (2014) 1444-1459.
[43] J. Bugler, K.P. Somers, E.J. Silke, H.J. Curran, Revisiting the kinetics and thermodynamics of the low-temperature oxidation pathways of alkanes: A case study of the three pentane isomers, J. Phys. Chem. A 119 (2015) 7510-7527.
[44] S.W. Benson, Thermochemical kinetics, Wiley, 1976.
[45] S.M. Burke, J.M. Simmie, H.J. Curran, Critical evaluation of thermochemical properties of C1-C4 species: updated group-contributions to estimate thermochemical properties, J. Phys. Chem. Ref. Data 44 (2015) 29.
[46] E.R. Ritter, J. Bozzelli, THERM: Thermodynamic property estimation for gas phase radicals and molecules, Int. J. Chem. Kinet. 23 (1991) 767-778.
[47] W.H. Green, J.W. Allen, R.W. Ashcraft, G.J. Beran, C.A. Class, C. Gao, C.F. Goldsmith, M.R. Harper, A. Jalan, G.R. Magoon, D.M. Matheu, S.S. Merchant, J.D. Mo, S. Petway, S. Raman, S. Sharma, J. Song, K.M. Van Geem, J. Wen, R.H. West, A. Wong, H. Wong, P.E. Yelvington, J. Yu, RMG-Reaction Mechanism Generator v3.3 2011, <http://rmg.sourceforge.net/>.
[48] H.J. Curran, Developing detailed chemical kinetic mechanisms for fuel combustion, Proc. Combust. Inst. 37 (2019) 57-81.
[49] S.J. Klippenstein, Y. Georgievskii, L.B. Harding, Predictive theory for the combination kinetics of two alkyl radicals, Phys. Chem. Chem. Phys. 8 (2006) 1133-1147.
[50] F. Zhang, Z. Wang, Z. Wang, L. Zhang, Y. Li, F. Qi, Kinetics of decomposition and isomerization of methylcyclohexane: Starting point for studying monoalkylated cyclohexanes combustion, Energy Fuels 27 (2013) 1679-1687.
[51] L.B. Harding, Y. Georgievskii, S.J. Klippenstein, Predictive theory for hydrogen atom - Hydrocarbon radical association kinetics, J. Phys. Chem. A 109 (2005) 4646-4656.
[52] R. Sivaramakrishnan, J.V. Michael, Rate constants for OH with selected large alkanes: Shock-tube measurements and an improved group scheme, J. Phys. Chem. A 113 (2009) 5047-5060.
[53] R. Sivaramakrishnan, N.K. Srinivasan, M.C. Su, J.V. Michael, High temperature rate constants for OH+ alkanes, Proc. Combust. Inst. 32 (2009) 107-114.
[54] R. Sivaramakrishnan, J.V. Michael, Shock tube measurements of high temperature rate constants for OH with cycloalkanes and methylcycloalkanes, Combust. Flame 156 (2009) 1126-1134.
[55] H.-H. Carstensen, A.M. Dean, O. Deutschmann, Rate constants for the H abstraction from alkanes (R–H) by R′O2 radicals: A systematic study on the impact of R and R′, Proc. Combust. Inst. 31 (2007) 149-157.
[56] J. Aguilera-Iparraguirre, H.J. Curran, W. Klopper, J.M. Simmie, Accurate benchmark calculation of the reaction barrier height for hydrogen abstraction by the hydroperoxyl radical from methane. Implications for CnH2n+2 where n=2→4, J. Phys. Chem. A 112 (2008) 7047-7054.
[57] J.P. Orme, H.J. Curran, J.M. Simmie, Experimental and modeling study of methyl cyclohexane pyrolysis and oxidation, J. Phys. Chem. A 110 (2006) 114-131.
[58] B.W. Weber, W.J. Pitz, M. Mehl, E.J. Silke, A.C. Davis, C.-J. Sung, Experiments and modeling of the autoignition of methylcyclohexane at high pressure, Combust. Flame 161 (2014) 1972-1983.
[59] W. Tsang, J.A. Walker, J.A. Manion, The decomposition of normal hexyl radicals, Proc. Combust.

Inst. 31 (2007) 141-148.
[60] W.S. McGivern, I.A. Awan, W. Tsang, J.A. Manion, Isomerization and decomposition reactions in the pyrolysis of branched hydrocarbons: 4-Methyl-1-pentyl radical, J. Phys. Chem. A 112 (2008) 6908-6917.
[61] W. Tsang, W.S. McGivern, J.A. Manion, Multichannel decomposition and isomerization of octyl radicals, Proc. Combust. Inst. 32 (2009) 131-138.
[62] B. Sirjean, E. Dames, H. Wang, W. Tsang, Tunneling in hydrogen-transfer isomerization of n-alkyl radicals, J. Phys. Chem. A 116 (2012) 319-332.
[63] B. Sirjean, P.A. Glaude, M.F. Ruiz-Lopez, R. Fournet, Theoretical kinetic study of thermal unimolecular decomposition of cyclic alkyl radicals, J. Phys. Chem. A 112 (2008) 11598-11610.
[64] Y. Yang, A.L. Boehman, Experimental study of cyclohexane and methylcyclohexane oxidation at low to intermediate temperature in a motored engine, Proc. Combust. Inst. 32 (2009) 419-426.
[65] Y. Yang, A.L. Boehman, Oxidation chemistry of cyclic hydrocarbons in a motored engine: Methylcyclopentane, tetralin, and decalin, Combust. Flame 157 (2010) 495-505.
[66] Y. Yang, A.L. Boehman, J.M. Simmie, Uniqueness in the low temperature oxidation of cycloalkanes, Combust. Flame 157 (2010) 2357-2368.
[67] Y. Yang, A.L. Boehman, J.M. Simmie, Effects of molecular structure on oxidation reactivity of cyclic hydrocarbons: Experimental observations and conformational analysis, Combust. Flame 157 (2010) 2369-2379.
[68] A. Miyoshi, Molecular size dependent falloff rate constants for the recombination reactions of alkyl radicals with O2 and implications for simplified kinetics of alkylperoxy radicals, Int. J. Chem. Kinet. 44 (2012) 59-74.
[69] R.X. Fernandes, J. Zador, L.E. Jusinski, J.A. Miller, C.A. Taatjes, Formally direct pathways and low-temperature chain branching in hydrocarbon autoignition: the cyclohexyl + O2 reaction at high pressure, Phys. Chem. Chem. Phys. 11 (2009) 1320-1327.
[70] A.M. Knepp, G. Meloni, L.E. Jusinski, C.A. Taatjes, C. Cavallotti, S.J. Klippenstein, Theory, measurements, and modeling of OH and HO2 formation in the reaction of cyclohexyl radicals with O2, Phys. Chem. Chem. Phys. 9 (2007) 4315-4331.
[71] J. Zou, X. Zhang, Y. Li, L. Ye, L. Xing, W. Li, C. Cao, Y. Zhai, F. Qi, J. Yang, Experimental and kinetic modeling investigation on ethylcyclohexane low-temperature oxidation in a jet-stirred reactor, Combust. Flame 214 (2020) 211-223.
[72] X. Yao, J. Wang, Q. Yao, Y. Li, Z. Li, X. Li, Pressure-dependent rate rules for intramolecular H-migration reactions of normal-alkyl cyclohexylperoxy radicals, Combust. Flame 204 (2019) 176-188.
[73] J.A. Miller, S.J. Klippenstein, S.H. Robertson, A theoretical analysis of the reaction between ethyl and molecular oxygen, Proc. Combust. Inst. 28 (2000) 1479-1486.
[74] E.G. Estupiñán, J.D. Smith, A. Tezaki, S.J. Klippenstein, C.A. Taatjes, Measurements and modeling of DO2 formation in the reactions of C2D5 and C3D7 radicals with O2, J. Phys. Chem. A 111 (2007) 4015-4030.
[75] S.M. Villano, L.K. Huynh, H.H. Carstensen, A.M. Dean, High-pressure rate rules for alkyl + O2 reactions. 1. The dissociation, concerted elimination, and isomerization channels of the alkyl peroxy radical, J. Phys. Chem. A 115 (2011) 13425-13442.
[76] Z. Wang, D.M. Popolan-Vaida, B. Chen, K. Moshammer, S.Y. Mohamed, H. Wang, S. Sioud, M.A. Raji, K. Kohse-Hoinghaus, N. Hansen, P. Dagaut, S.R. Leone, S.M. Sarathy, Unraveling the structure and chemical mechanisms of highly oxygenated intermediates in oxidation of organic compounds, Proc.

Natl. Acad. Sci. U.S.A. 114 (2017) 13102-13107.
[77] C.F. Goldsmith, W.H. Green, S.J. Klippenstein, Role of O2+QOOH in low-temperature ignition of propane. 1. Temperature and pressure dependent rate coefficients, J. Phys. Chem. A 116 (2012) 3325-3346.
[78] S.M. Villano, L.K. Huynh, H.H. Carstensen, A.M. Dean, High-pressure rate rules for alkyl + O2 reactions. 2. The isomerization, cyclic ether formation, and beta-scission reactions of hydroperoxy alkyl radicals, J. Phys. Chem. A 116 (2012) 5068-5089.
[79] L. Xing, L. Zhang, F. Zhang, J. Jiang, Theoretical kinetic studies for low temperature oxidation of two typical methylcyclohexyl radicals, Combust. Flame 182 (2017) 216-224.
[80] Walker, R. W. Morley, C. Oxidation kinetics and autoignition of hydrocarbons. In Comprehensive Chemical Kinetics. Pilling, M. J., Ed. Elsevier: New York, 1997.
[81] T. Bissoonauth, Z. Wang, S.Y. Mohamed, J.-y. Wang, B. Chen, A. Rodriguez, O. Frottier, X. Zhang, Y. Zhang, C. Cao, J. Yang, O. Herbinet, F. Battin-Leclerc, S.M. Sarathy, Methylcyclohexane pyrolysis and oxidation in a jet-stirred reactor, Proc. Combust. Inst. 37 (2019) 409-417.
[82] M. Liu, R. Fang, C.-J. Sung, C. Yan, Y. Ju, J. Zhao, Z. Tao, C.-W. Zhou, A comprehensive study of n-propylcyclohexane three-stage auto-ignition at low temperature, (2021, submitted to Combustion and Flame).